In Pursuit of a Selective Hepatocellular Carcinoma Therapeutic Agent: Novel Thalidomide Derivatives with Antiproliferative, Antimigratory and STAT3 Inhibitory Properties

Michael J. Nutt,[a, b] Yeung Sing Yee,[a] Amanda Buyan,[c] Neil Andrewartha,[a, b] Ben Corry,[c] George C.T. Yeoh,[a, b*] Scott G. Stewart.[a*]

[a] School of Molecular Sciences, The University of Western Australia, Crawley, WA 6009, Australia
[b] The Centre for Medical Research, The Perkins Institute of Medical Research, Nedlands, WA 6009, Australia
[c] Research School of Biology, Australian National University, Acton, ACT, 2601, Australia.

Abstract: Advanced stage liver cancer is predominantly treated with the multi-kinase inhibitor sorafenib, however this therapeutic agent lacks selectivity in its cytotoxic actions and is associated with poor survival outcomes. Herein we report the design and preparation of several thalidomide derivatives, including a variety of novel thioether-containing forms that are especially rare in the literature. Importantly, two of the derivatives described are potent antiproliferative agents with dose-dependent selectivity for tumorigenic liver progenitor cells (LPC) growth inhibition (up to 36% increase in doubling time at 10 μM) over non-tumorigenic cells (no effect at 10 μM). Furthermore, these putative anti-liver cancer agents were also found to be potent inhibitors of tumorigenic LPC migration. This report also describes these derivatives' effects on several key signalling pathways in our novel liver cell lines by immunofluorescence and AlphaLISA assays. Aryl thioether derivative **7f** significantly reduced STAT3 phosphorylation (23%) and nuclear localisation (16%) at 10 μM in tumorigenic LPCs, implicating the IL-6/JAK/STAT3 axis in the mode of action of our derivatives.

Introduction:

In the last 20 years a resurgence of thalidomide use in drug therapy has uncovered interesting and desirable biological activities including enhanced T-cell stimulation and proliferation, as well as anti-tumour and anti-angiogenic effects.[1–3] Furthermore, thalidomide and its derivatives (lenalidomide, pomalidomide, avadomide, iberdomide, and CC-885 from Celgene, Figure 1) can modulate the immune response in several cell types, as well as indirectly influence cell signalling pathways involved in growth, proliferation, and apoptosis.[4–6] Currently, this family of drugs has approved uses for treating a range of disease states including multiple myeloma (MM), 5q deletion-associated myelodysplastic syndrome (MDS), erythema nodosum leprosum (ENL) and psoriatic arthritis.[7–9]

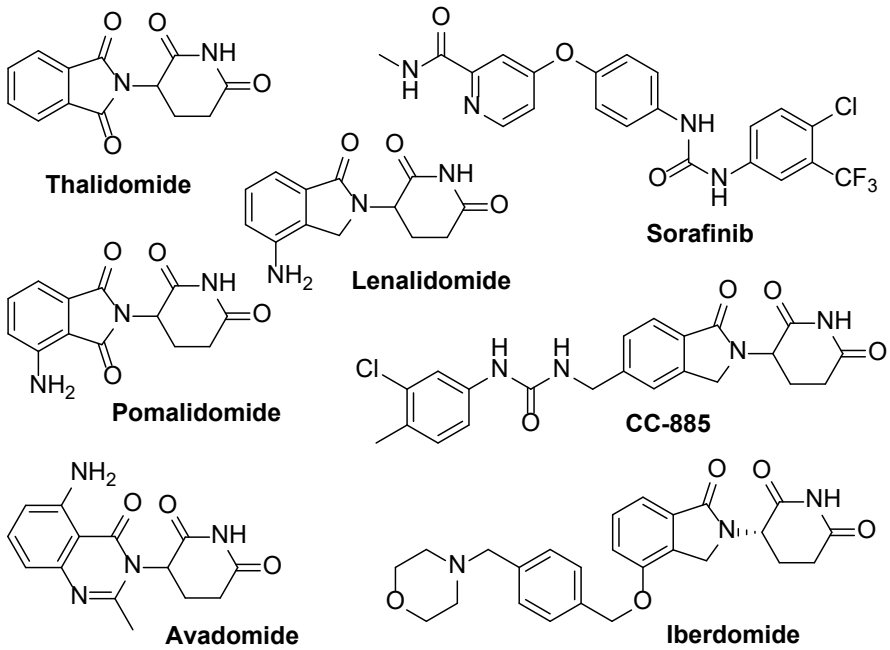

Figure 1. Structure of thalidomide, sorafenib, and thalidomide derivatives developed by Celgene.

For decades the mechanism(s) underlying thalidomide's pleiotropic biological activities remained unclear, and presumed the involvement of multiple distinct drug targets.[10] In 2010 however, a landmark paper from the Ito group revealed cereblon (CRBN) as the primary target of thalidomide, and furthermore was responsible for its teratogenic effects in early-term pregnancies. CRBN forms part of an E3 ubiquitin ligase complex (known collectively as $CRL4^{CRBN}$) that regulates proteosomal degradation *via* substrate ubiquitination, and upon binding of thalidomide to CRBN substrate specificity of the ligase activity is altered, inducing protein degradation of downstream targets.[11,12] While originally described as immunomodulatory drugs (IMiDs), thalidomide and its derivatives are now also referred to as CELMoDs (cereblon modulators), to better reflect this more detailed mechanism of action.

In the last decade, protein crystallography studies have revealed the CRBN binding site of thalidomide and other CELMoDs, to be highly conserved between species from bacterial to mammalian.[13,14] It is now known that the glutarimide ring shared by these compounds is essential for CRBN binding affinity, while the phthaloyl scaffold remains partially exposed where it forms part of the protein-protein interface between CRBN and the target of ubiquination.[15–17] Unique neosubstrates of CRBN have been identified that mediate both the therapeutic effects of these drugs in MM (the zinc finger transcription factors IKZF1 and IKZF3) and MDS (the serine/threonine kinase CK1α), as well as some of thalidomide's maligned birth defects (SALL4, another zinc finger).[18] The ability to induce degradation of these targets differs between each member of the CELMoD class, and thus it is now understood that subtle structural differences in the substitution at the phthaloyl ring can create various opportunities for further intermolecular interactions that reflect their unique degradation profiles.[19]

While thalidomide and some derivatives have been especially successful in treating hematological malignancies, reports of their use in the treatment of HCC is rare in the literature.[20–23] Hepatocellular carcinoma is an especially lethal disease: estimates place it as the sixth most common cancer, and yet responsible for the fourth highest number of cancer-related deaths worldwide.[24,25] Liver cancers are notoriously resistant to chemotherapeutic agents due to the liver's inherent ability to rapidly metabolise and efflux exogenous agents. Partial liver

resection or transplant are the only potentially curative options for HCC patients, but require sufficiently early diagnosis. Only seven drugs currently hold FDA approval for the treatment of HCC, including first-line choice Sorafenib (Figure 1), which unfortunately suffers from poor selectivity and provides only modest improvements to median patient survival *i.e.* 3 months in clinical trials.[26,27] There is thus a pressing need for the development of improved chemotherapeutic agents for the treatment of HCC.

Our research team's establishment of a liver progenitor cell (LPC) line designated BMOL (for Bipotential Mouse Oval Liver) provides a unique platform for compound evaluation.[22,28] The ability for BMOL cells to differentiate into both cholangiocytes and hepatocytes in culture confirms their progenitor cell status by function. In the context of this communication, their association with liver pathologies and cancer is significant: reports suggest some forms of HCC are derived from LPCs, and it is also claimed some LPCs may function as liver cancer stem cells.[29–33] Extensive passage of some of these cell lines, including BMOL cells, generates tumorigenic (T) cell lines from what are originally non-tumorigenic (NT).[22,28] This methodology provides a novel approach to assess both selectivity and efficacy in our screens by comparing responses in matched pairs of BMOL-NT cells versus BMOL-T cells. Our early structure-activity relationship (SAR) studies of thalidomide analogues in TNFα expression inhibition and apoptosis studies highlighted several analogues which had higher potency than thalidomide and lenalidomide.[34–36] Suppression of TNFα expression is a well-documented property of the IMiDs, and its role in HCC warranted study of our derivatives as potential therapeutic agents.[37–39] In a preliminary investigation we recently identified a standout aryl amine-bearing thalidomide analogue which inhibited the growth of tumorigenic hepatocytes without affecting BMOL-NT cell growth.[22] The present work seeks to discover related compounds with improved anticancer potency while maintaining the desired selectivity for tumorigenic liver cells. We also seek to understand its mechanism of action by identifying signalling pathways involved in this selective growth inhibition. The potential role of CRBN binding in eliciting these actions is also examined both experimentally and through molecular dynamics (MD) simulation approaches.

Results and discussion:

Chemistry. As a preliminary focus for our structure modifications, we prepared thalidomide derivatives functionalised at the C4 position with a range of atoms including C, N, S and O. As we have demonstrated in previous work, a library of thalidomide analogues could be obtained through cross-coupling techniques from appropriately halogenated thalidomide precursors (Scheme 1).[34] Thus, readily available 2,3-dimethylaniline (**1**) was first converted efficiently to 3-iodophthalic anhydride (**3**), which is subsequently condensed with the trifluoroacetic acid salt of aminoglutarimide to afford 4-iodothalidomide **4a** in 41% overall yield (4 steps).[40] This precursor could be conveniently prepared on a multi-gram scale and served as a key intermediate to several classes of thalidomide analogues. Similarly, application of this condensation to the commercially available brominated anhydride **3b** afforded 5-bromothalidomide **4b** in 68% yield (Scheme 1). Given the success of the commercial thalidomide derivatives lenalidomide and pomalidomide (Figure 1) and recent results within ours and other groups, a synthetic pathway for access to C4 nitrogen linked compounds was required. Fortunately, robust in-house conditions previously optimised for Buchwald-Hartwig aminations of our halogenated thalidomide precursors could be applied in these examples.[36] Using the precatalyst $Pd_2(dba)_3.CHCl_3$ and the biphenyl ligand XPhos, a coupling between iodothalidomide **4a** and aniline to **5a** could be achieved 97% yield (Scheme 1). Coupling of bromothalidomide **4b** in an analogous fashion required only half the catalytic loading to give **5c** in near-quantitative yield (99%).

The C4-benzyl functionalised analogue **5e** was accessed through a Suzuki-Miyaura cross-coupling between benzylboronic acid pinacol ester and **4a** in good yield (67%, Scheme 1). This approach was not amenable for the equivalent C4-ether-bridged isostere **5g** proved unobtainable through both palladium cross-coupling and copper-catalyzed Ullmann-type approaches. Instead, attaching the desired phenoxy-substituent onto the phthalimide scaffold was completed firstly through a S_NAr reaction between 3-fluorophthalic anhydride (**4c**) and phenol to furnish ether **4d** (Scheme 1),[41] which was subsequently reacted with the trifluoroacetate salt of glutarimide to provide ether **5g** (28% yield over two steps, Scheme 1).

The related C4-sulfur linked derivative was prepared in excellent yield (94%) through a C-S cross-coupling reaction of iodothalidomide **4** and thiophenol, using the catalyst system of $Pd_2(dba)_3{\cdot}CHCl_3$ and Xantphos (Scheme 1).[42] Thioether-containing derivatives of thalidomide are especially rare in the literature, where previously lenalidomide was subjected to a S-transfer reaction[43] and more recently *via* a photocatalysed approach.[44] This work is the first report of Pd-catalysed C-S cross-coupling to afford thalidomide thioethers, and complements the other recent approaches developed elsewhere. Initially, as the *para*-isopropyl amine **5b** was considered a starting point for this study,[22] each of the synthetic procedures outlined was also repeated to afford the *para*-isopropyl derivatives **5b**, **5f**, **5h** and **5j**. In the case of ispropyl-bearing thioether **5j** treatment under strong oxidative conditions (*m*-CPBA) also provided the corresponding desired sulfonyl analogue (**5k**) in 58% (Scheme 1).

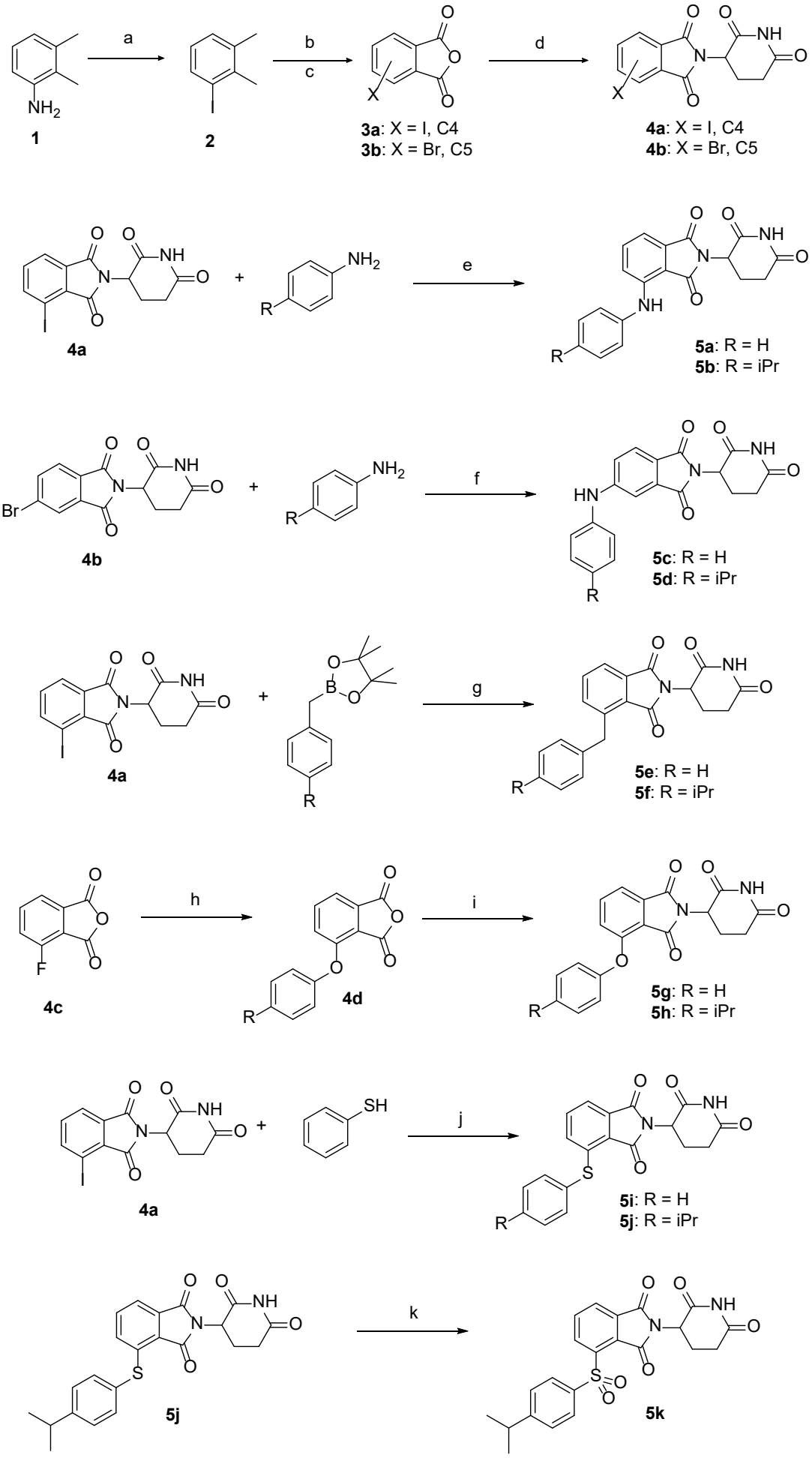
a
b
c
d
e
f
g
h
i
j
k
1
2
3a: X = I, C4
3b: X = Br, C5
4a: X = I, C4
4b: X = Br, C5
4a
4b
4c
4d
5a: R = H
5b: R = iPr
5c: R = H
5d: R = iPr
5e: R = H
5f: R = iPr
5g: R = H
5h: R = iPr
5i: R = H
5j: R = iPr
5j
5k

Scheme 1. *Reagents and Conditions*: a) $NaNO_2$, HCl, -5 °C then KI, 62%; b) $KMnO_4$, H_2O/pyridine, reflux, 24 h, 87%; c) Ac_2O, reflux, 22 h, 79%; d) glutarimide trifluoracetate, NEt_3, THF, reflux, 72 h, 73%; e) aniline (1.5 equiv), $Pd_2(dba)_3{\cdot}CHCl_3$ (4 mol%), XPhos (16 mol%), K_2CO_3 (2 equiv), 1,4-dioxane, reflux, 18 h; f) aniline (1.5 equiv), $Pd_2(dba)_3{\cdot}CHCl_3$ (2 mol%), XPhos (8 mol%), K_2CO_3 (2 equiv), 1,4-dioxane, reflux, 18 h; g) $Pd_2(dba)_3{\cdot}CHCl_3$ (8%) PPh_3 (1 equiv), Ag_2O, THF, 70 °C, 24h; h) phenol, KF, DMF; i) glutarimide trifluoroacetate, NEt_3, THF, reflux, 72 h,; j) thiophenol, $^iPr_2NEt$ (2 equiv), $Pd_2(dba)_3{\bullet}CHCl_3$ (2.5 mol%), Xantphos (5 mol%), 1,4-dioxane (2 mL), reflux, 14 h; k) *m*-CPBA (3 equiv), DCM, rt, 24 h, 58%.

The versatile nature of this outlined amination process allowed for the coupling of various electronically diverse anilines to functionalised thalidomide analogues in yields ranging from 15% to 98% (Scheme 2). A further 15 analogues were obtained for biological study with this approach, featuring both electron-rich (e.g. alkoxy and dimethylamino substituents) and electron deficient (e.g. trifluoromethyl, acetyl and ethyl ester motifs) *para*-substitued examples. The general coupling conditions could also be carried out with *ortho*-aminopyridine, *ortho*-toluidine and 2-aminotetralin to furnish compounds **7a** (90%), **7b** (58%) and **7h** (72%) respectively.

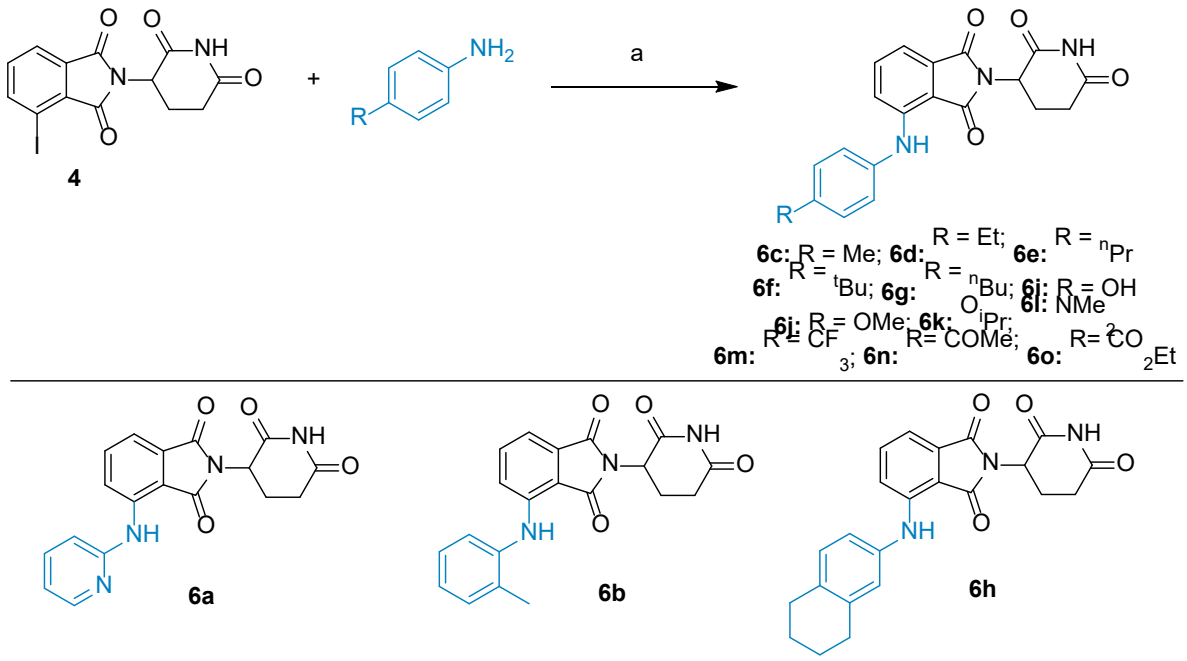

Scheme 2. *General Reagents and Conditions:* a) aniline (1.5 equiv), $Pd_2(dba)_3{\cdot}CHCl_3$ (4 mol%), XPhos (16 mol%), K_2CO_3 (2 equiv), 1,4-dioxane, reflux, 18 h, 15-99%.

In the case of the C-S cross-coupling, a diverse set of 14 thioether-linked analogues of thalidomide were prepared in yields ranging from fair to near-quantitative (Scheme 3). These reactions produced diaryl derivatives of thalidomide including *tert*-butyl (**7f**, 97%), methoxy (**7i**, 72%) and those bearing an electron-withdrawing substituent such as CF_3 (**7g**, 70%). It was suspected that the low yield of thioanisole **7j** (38%) resulted from undesired Pd-catalysed C-S cleavage of its methyl sulfide group, a process which has been reported previously.[45] Interestingly, more diverse thioethers could be produced under these robust cross coupling conditions such as those thalidomide analogues bearing *N*-heterocycles (**7a-b** and **7h**) and linear (**7l**) or bulky (**8m-o**) alkyl variants. Overall this approach was deemed an efficient and

high-yielding approach to thioether-linked derivatives of thalidomide, which complements other existing approaches that have recently been disclosed.[43,46] In addition to these cross-coupling products, a late-stage functionalisation of compound **7f** was performed by treatment with methyl iodide to give *N*-methylated analogue **7p** in excellent yield (Scheme 4).

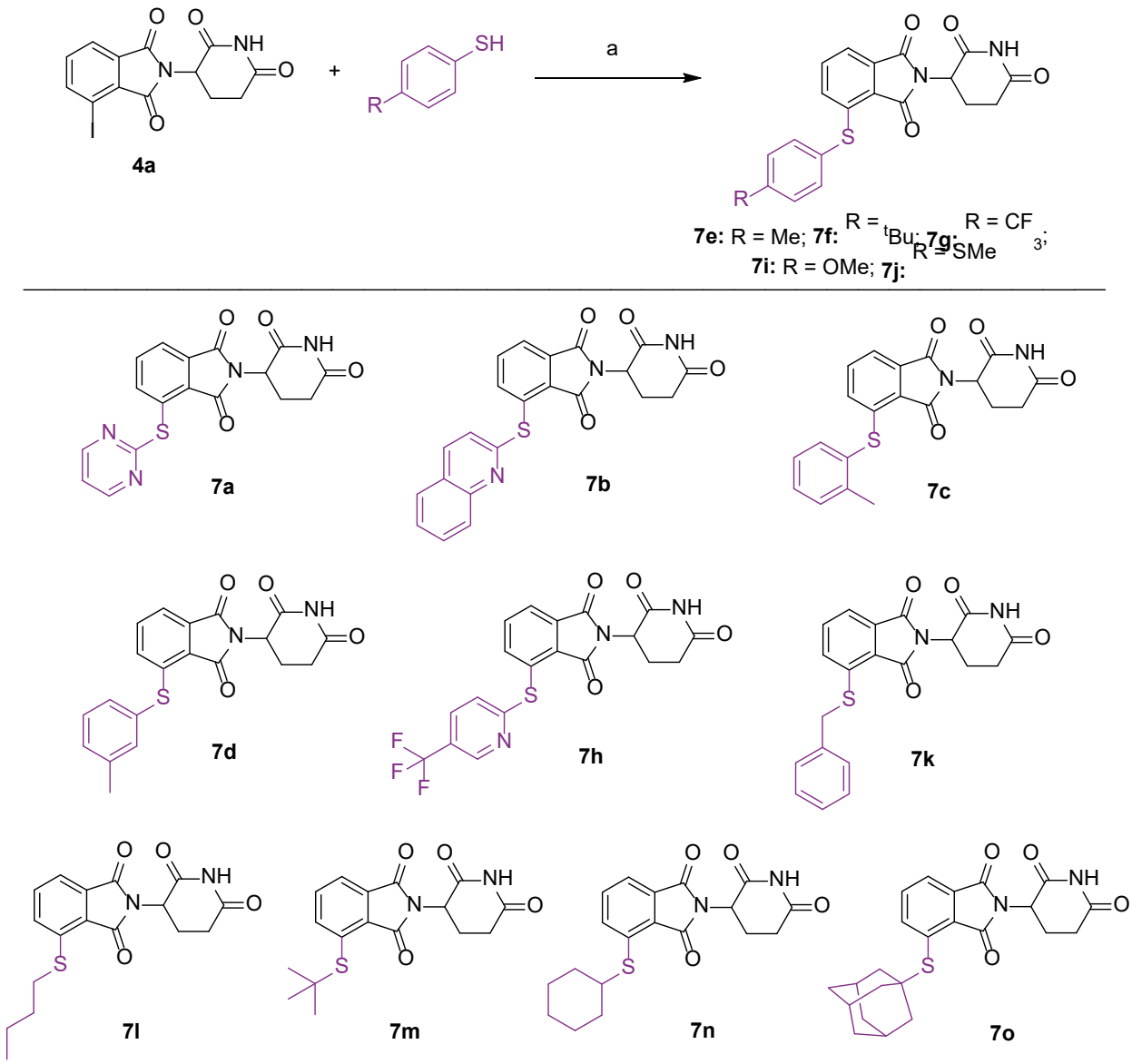

Scheme 3. *General Reagents and Conditions*: a) generic thiophenol or thiol, $^{i}Pr_2NEt$ (2 equiv), $Pd_2(dba)_3$**.**$CHCl_3$ (2.5 mol%), XantPhos (5 mol%), dioxane (2 mL), reflux, 14 h, 38-99%.

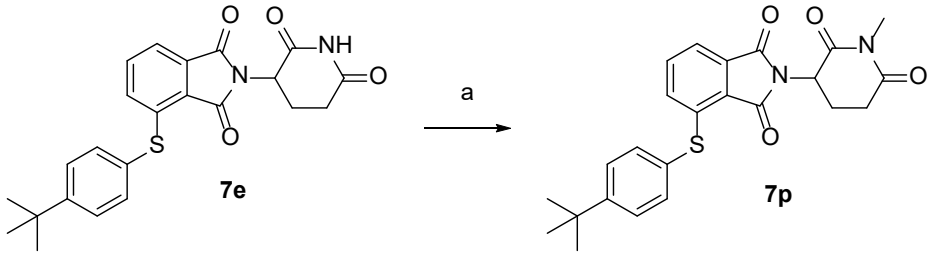

Scheme 4. *Reagents and Conditions*: a) MeI (1.2 equiv), K_2CO_3 (2 equiv), DMF, 0 °C – rt, 18 h, 95%.

Selective targeting of tumorigenic cell growth. To identify agents with selective antiproliferative effects in liver cancer cells, we screened for growth inhibition in a matched pair of BMOL-T/BMOL-NT cell lines established from the same lineage. The Incucyte Zoom (Essen BioScience) live-cell analysis system was used to monitor cell growth in real-time. In contrast to traditional end-point assessments of proliferation (such as the more common MTT assay), this platform offers dynamic real-time measurements of cell growth across the entire course of an experiment. The doubling time of each cell population during treatment can then be determined specifically during the log phase of cell growth. We had previously established selective antiproliferative activity of **5b** in these cell lines at a 10 μM concentration.[22] This extension of the previous study seeks to identify novel derivatives of **5b** with enhanced efficacy at this dose, while maintaining selectivity for the BMOL-T cell line. Concurrently we sought to elucidate SARs which could be used as tools to predict this selectivity, to better inform drug design approaches. Structural modifications to the aromatic phthalimide ring have led to improved multiple myeloma activity through initial CRBN binding and further interaction with the IKAROS family of lymphocyte transcription factors (IKZF1/3).[47] Thus, we hoped to determine if variation in aromatic substitution could result in an improvement in activity in BMOL cell models.

To first establish a baseline response in the BMOL cell lines used in this study, treatments of 10 μM with either thalidomide, lenalidomide, pomalidomide, or sorafenib (Figure 1) were used in the Incucyte proliferation assay (Table 1). At 10 μM concentration, only sorafenib produced any statistically significant effect on the growth of either cell line. While increasing doubling time for BMOL-T cells (2.1-fold greater than that of the NT line) sorafenib nevertheless demonstrated severe antiproliferative activity in BMOL-NT cells. In contrast, at the same dose our previously described derivative **5b** was able to inhibit BMOL-T growth without any concomitant effect on NT cell growth.[22] Interestingly, thalidomide and its derivatives were well-tolerated by both cell lines, and were completely inactive as antiproliferative agents at this dose. These findings are in accordance with both evidence from clinical trials[48] and our own prior work[22] in these cell lines, where no effect on BMOL cell growth was observed at 10 μM, and at higher (100 μM) doses only indiscriminate growth inhibition of both T and NT cell lines equally was observed. This also held true for pomalidomide which to our knowledge has never been assessed for inhibitory activity in liver cancer. Furthermore, this data suggests that the structural modifications introduced in our thalidomide derivative **5b** are required for anticancer activity in these cell lines, and that the parent drug does not share its selective activity against BMOL-T proliferation.

Table 1: Differential effects of several commercial drugs on growth inhibition of BMOL-NT and BMOL-T cells. Growth is reported as mean doubling times in hours *(n* = 3 in all cases, with SEM in parentheses), control represents 0.1% DMSO vehicle in supplemented growth medium. Statistical significance is indicated as follows: * = $p < 0.05$, ** = $p < 0.01$, *** = $p < 0.001$.

	BMOL-NT			**BMOL T**		
Treatment	Growth *(SEM)*	Change Over Control	*p*	Growth *(SEM)*	Change Over Control	*p*
Control	18 *(0.4)*	-	NS	15 *(0.3)*	-	NS
Thalidomide	18 *(0.3)*	-	NS	15 *(0.6)*	-	NS
Pomalidomide	18 *(0.2)*	-	NS	15 *(0.5)*	-	NS
Lenalidomide	18 *(0.6)*	-	NS	15 *(0.5)*	-	NS

Sorafenib	50 *(8.2)*	**181%**	***	71 *(7.6)*	**382%**	***

In the case of TNF inhibition, C4-amine substituted lenalidomide is much more potent than its C5-amino analogue – a trend we have also identified in the TNF inhibition profiles of our amine-derived compounds previously.[36,49] Nevertheless, given the aniline derived **5b** exhibited selective cell growth inhibition, the equivalent C5-substituted compound was considered in this current study to confirm the optimal position of substitution (Table 2). Additionally, to examine any contribution of the bridging aniline nitrogen atom to the observed efficacy and selectivity of **5b** against HCC, we sought isosteric and analogous compounds. Thus, derivatives featuring methylene-, oxygen- and sulfur-bridged aryl groups were also subjected to our cell growth assays at a 10 μM dose (Table 2). Remarkably, the *para*-isopropyl examples of benzyl, thioether and aniline derivatives (**5b**, **5f** and **5j**) all demonstrated near-identical levels of cancer growth inhibition, and all three remained selective towards the BMOL-T line. Each of these functionalities offer a unique set of hydrogen bonding capacities (**5b** as acceptor and donor, **5i** as acceptor only, and **5e** with none at all), and the homogeneity of their responses in BMOL cells indicates that hydrogen bonding between this site and a potential cellular target plays no role in our compounds' efficacy. This tolerance of various bridging atoms was not without limits, however: both ethers (**5g-h**) and sulfonyl (**5k**) derivatives failed to elicit growth inhibition in either liver cell line. This, taken together with the apparent requirement of ^{i}Pr substitution for selective growth inhibition may indicate a general preference for compounds with higher lipophilicity. Notably, moving substituent to the adjacent C5 position and removal of the ^{i}Pr moiety both ablated antiproliferative activity (compound **5a**) – a result mirrored in both benzyl and thioether derivatives. Thus, this early study revealed examples of benzyl, amine, and sulfide derivatives of thalidomide (**5f**, **5b**, and **5j** respectively), each differing in their H-bonding donor and acceptor capacities, were found to be selective BMOL-T growth inhibitors. Furthermore, exchange of these successful linkers with either sulfonyl or ether functionalities was not tolerated, and the *para*-isopropyl aryl group was deemed essential for more potent cell growth inhibition. Each of these factors was next examined carefully through a more thorough SAR investigation.

Table 2: Differential effects of thalidomide derivatives on growth inhibition of BMOL-NT and BMOL-T cells. Growth is reported as mean doubling times in hours *(n* = 3 in all cases, with SEM in parentheses), control represents 0.1% DMSO vehicle in supplemented growth medium. Statistical significance is indicated as follows: * = $p < 0.05$, ** = $p < 0.01$, *** = $p < 0.001$.

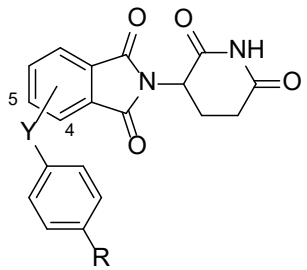

Compd.	Ring Position	Y	R	BMOL-NT Growth *(SEM)*	BMOL-NT % Change	BMOL-NT *p*	BMOL-T Growth *(SEM)*	BMOL-T % Change	BMOL-T *p*
5a	4	N	H	17.4 *(0.4)*	-	NS	14.3 *(0.4)*	**7%**	NS
5b	4	N	iPr	17.3 *(0.4)*	-	NS	16.3 *(0.7)*	**19%**	***
5c	5	N	H	17.4 *(0.1)*	-	NS	14.7 *(0.7)*	**4%**	NS
5d	5	N	iPr	17.2 *(0.4)*	-	NS	14.1 *(0.3)*	**3%**	NS

5e	4	C	H	17.7 *(0.9)*	**2%**	NS	13.8 *(0.5)*	**-**	NS
5f	4	C	iPr	17.5 *(0.3)*	**-**	NS	17.0 *(0.6)*	**17%**	***
5g	4	O	H	16.9 *(0.6)*	**-**	NS	14.3 *(0.2)*	**6%**	NS
5h	4	O	iPr	17.5 *(0.6)*	**-**	NS	15.4 *(0.3)*	**5%**	NS
5i	4	S	H	16.8 *(0.4)*	**1%**	NS	13.8 *(0.5)*	**2%**	NS
5j	4	S	iPr	17.2 *(0.8)*	**3%**	NS	16.2 *(1.1)*	**19%**	**
5k	4	SO_2	iPr	17.4 *(0.8)*	**3%**	NS	14.9 *(0.7)*	**3%**	NS

A range of compounds bearing modifications to the aminophenyl group were investigated for selective BMOL-T growth inhibition (Figure 2). Having already highlighted the importance of the isopropyl group contained within our previous lead, we sought to further optimise and investigate the importance of this unique substitution. Encouragingly, the only compound in this series to selectively inhibit growth of the non-tumorigenic cells (BMOL-NT) preferentially was the 2-pyridyl compound **6a** (10 μM). Introduction of a single methyl substituent alone to the phenyl ring was not enough to induce the activity observed in **5b**, and moreover the position of substitution (*ortho* vs. *para*; **6b** and **6c**) had negligible effect on compound potency or selectivity. Of the alkyl derived compounds related to ^{i}Pr-substituted compound **5b**, five derivatives (**6d** – **6h**) demonstrated comparable or greater growth inhibition towards tumourigenic cells at 10 μM. Chain length appeared to be a crucial factor determining selectivity; both the shorter ethyl chain of **6d** and the larger 4-carbon substituents of ^{n}Bu (**6g**) and tetralin (**6h**) derivatives introduced modest inhibition (up to 10%) of BMOL-NT proliferation. Negligible differences in activity and selectivity were observed when comparing the ^{i}Pr and ^{n}Pr analogues **5b** and **6e**, while the ^{t}Bu derivative **6f** was the most potent compound of all analogues in this series. Treatment of the BMOL cells with **6f** produced 31% inhibition of BMOL-T growth, with no concomitant decrease in BMOL-NT growth observed.

To determine whether the importance of alkyl substituent choice stemmed from its impact on compound lipophilicity or was instead governed by steric requirements for target binding, we calculated several physicochemical parameters of all novel compounds including LogP (see supporting information for these data). The calculated logP (cLogP) values of alkyl-substituted compounds **6c** – **6g** were in the range 1.56-3.45 (see supporting information for a summary of physicochemical parameters). High cLogP alone was not a reliable predictor of efficacy or selectivity however; ^{n}Buderivative **6g** (cLogP = 3.45) was less selective and no more potent than the isopropyl equivalent **5b** (cLogP = 2.93). These data imply that modulation of the overall compound lipophilicity is not wholly responsible for the observed selectivity and activity in antiproliferative actions of our alkyl-subsituted compounds against the BMOL line. Aniline derived thalidomide analogues with *para*-polar groups were designed to confirm this theory, and to probe whether H-bond acceptor/donors in this position could influence potency. Important to note was compounds bearing OH, OMe, O^{i}Pr, and NMe_2 groups were all inhibitors of BMOL-T growth and did not significantly affect BMOL-NT cells, though they proved less promising in selectivity and potency that the alkyl derivatives described above. It would appear from these results that H-bond donors or acceptors at this position are tolerated but do not improve activity. Diaryl amine thalidomide derivatives with carbonyl-containing moieties in this position were not effective in inhibiting cell growth. Promisingly, from this study seven new analogues (**6e-f** and **6h-l**) were identified as selective growth inhibitors of tumorigenic liver progenitor cells.

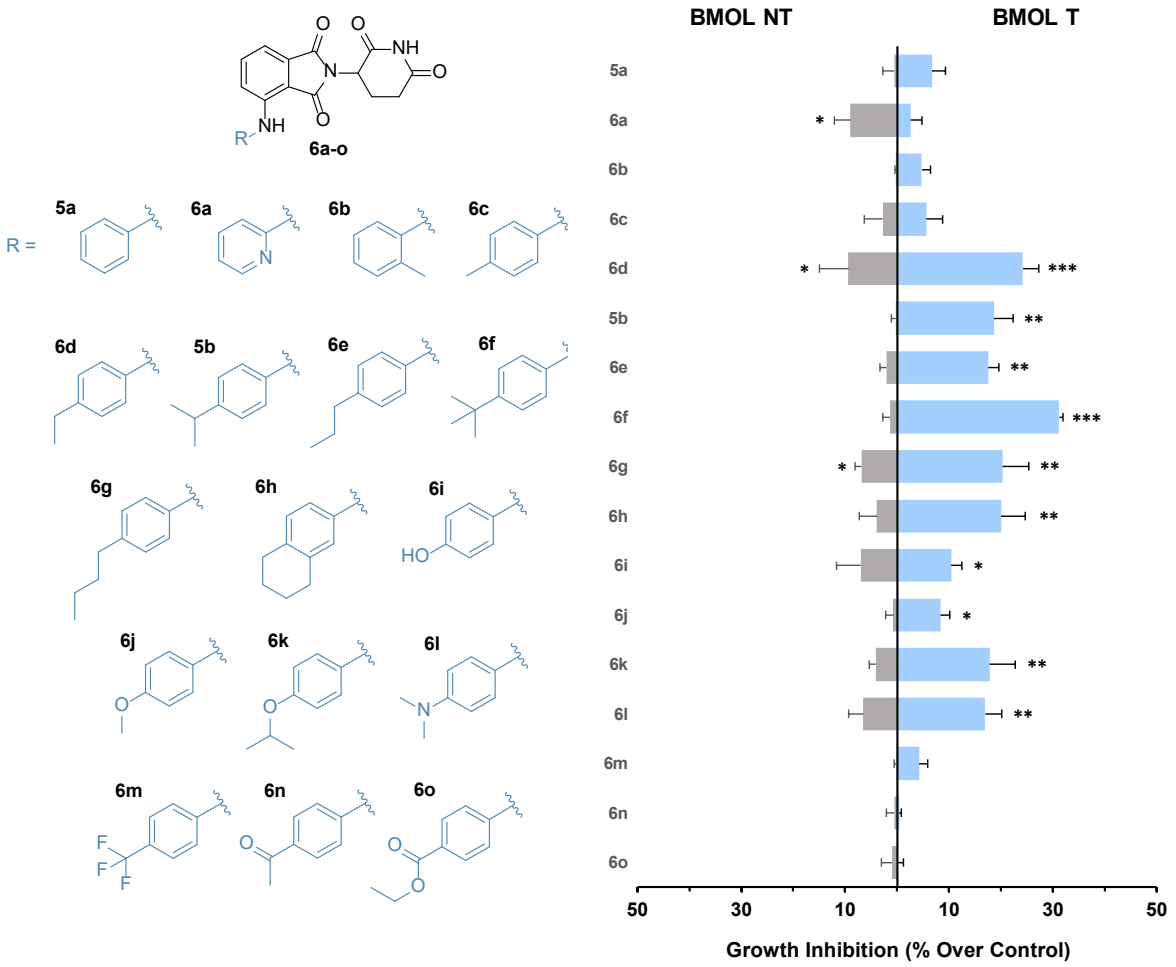

Figure 2: Aniline derived thalidomide derivatives and BMOL-T and BMOL-NT growth inhibition. Values reported as percentage change in mean doubling time over control for each cell line. Error bars represent SEM of three independent experiments. * = $p < 0.05$, ** = $p < 0.01$, *** = $p < 0.001$.

Following the improved growth inhibition displayed by compound **6f** a series of thioether-containing derivatives were also investigated (Figure 3). Overall, our thioether compounds showed less promise than the above aniline derived compounds. Similar profiles of activity were observed in those compounds with an aniline derived derivative bearing identical substituents (7**c**, **7e**, **7f-g**, and 7**i**) apart from anisole **7i** which was not consistently tolerated by BMOL-NT cells at this dose and exhibited some indiscriminate growth inhibition. The promising selectivity and potency of ^{i}Pr and ^{t}Bu substituted **7e-f** however proves that thioether motifs can serve equally as well as our amine candidates (Figure 2). ^{t}Bu thioether **7f** demonstrated remarkable selective activity, with 36% growth inhibition of the BMOL-T cell lines and no significant inhibition of the NT cell line. Importantly, **7f** has a 9-fold factor of selectivity for BMOL-T cells (compared to 2.1-fold for sorafenib as described in Table 1) and was the most potent compound identified in this study at the 10 µM dose. More polar isosteres of **7f** for example those featuring a *p*-CF_3 group (**7g-h**) failed to elicit any growth inhibition. Unfortunately, our set of aliphatic thioethers were also all poor inhibitors of growth, and no predictive trend was found between their lipophilicity and BMOL cell response (cLogP values ranged from 1.05-2.78). Interestingly, pyrimidine and quinoline derived compounds **7a-b** produced no measurable effect on BMOL-NT growth, unlike pyridyl aniline **6a** above. This

would suggest heterocycles may be incorporated into thalidomide thioether derivatives to further modulate drug properties such as solubility, without compromising overall selectivity in HCC.

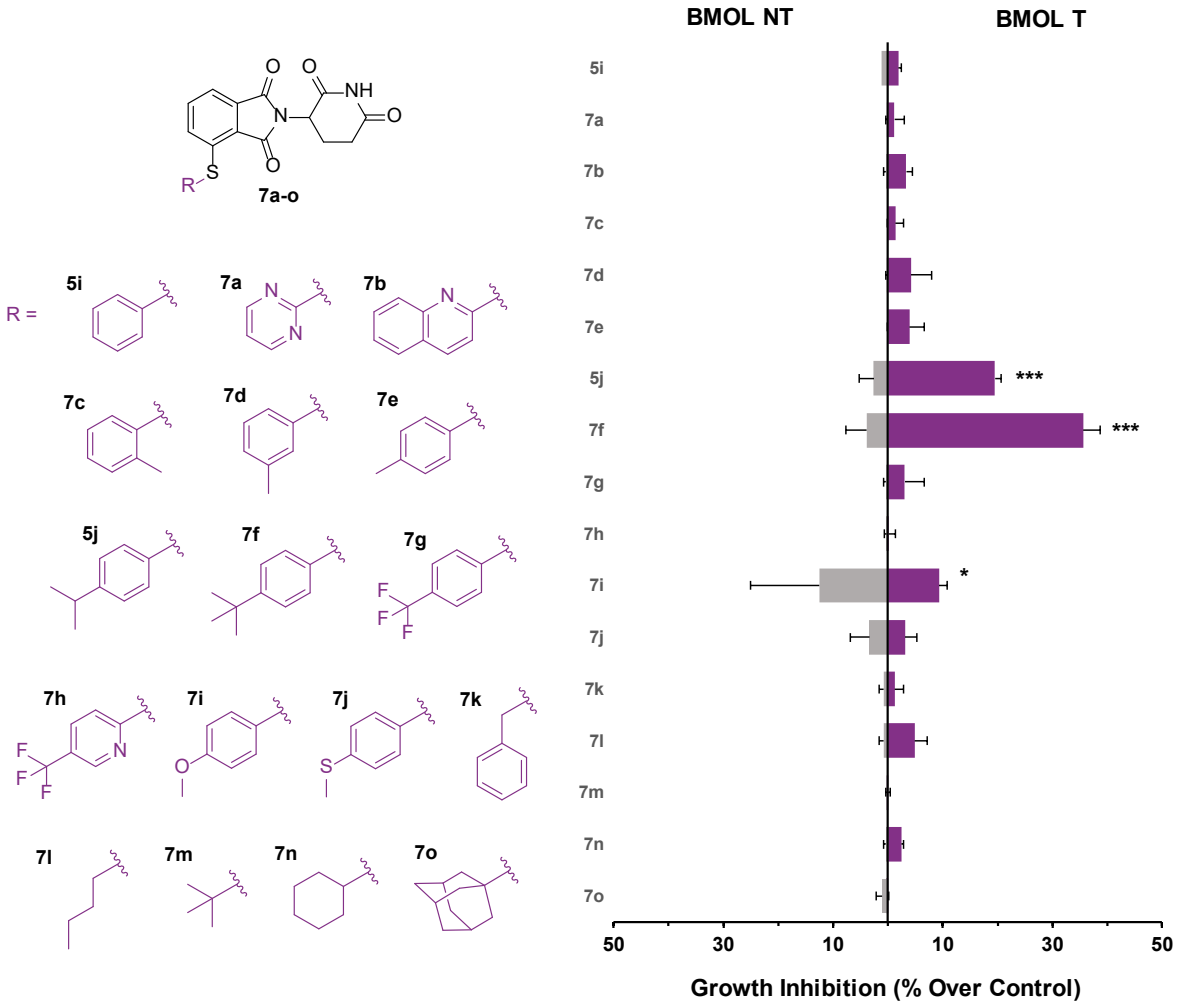

Figure 3: Sulfide derived thalidomide derivatives and BMOL-T and BMOL-NT growth inhibition. Values reported as percentage change in mean doubling time over control for each cell line. Error bars represent SEM of at least three independent experiments. * = $p < 0.05$, ** = $p < 0.01$, *** = $p < 0.001$.

Having identified ^{t}Bu-functionalised **6f** and **7f** as the most selective and potent in the class of amine and sulfide derivatives respectively, we set out to confirm that their effects were dose-dependent and identify the lowest active dose for each (Figure 4). Thioether **7f** was active at doses as low as 6 μM, while amine derivative **6f** remained active at the lowest tested concentration of 4 μM; half that of the lead compound **5b** in our previous study.[22] From this data we projected that at high enough doses, both compounds would begin to show the undesired inhibition of BMOL-NT cells and diminished selectivity. As expected, a clear dose-dependent increase in growth inhibition of BMOL-T cells was observed for both compounds. Furthermore, inhibition of non-tumorigenic cells occurred at all doses greater than 10 μM for both compounds – however, this inhibition was not dose-dependent for sulfide **7f** which remained essentially constant between doses of 14-26 μM. While amine **6f** was undoubtedly the more potent compound in BMOL-T cells, its reduced selectivity from 23-fold preference for BMOL-T at 10 μM, to 3-fold at the highest tested concentration, renders it less promising

than its sulfur analogue **7f**, which retains an excellent 9-fold selectivity at the higher concentration of 26 μM.

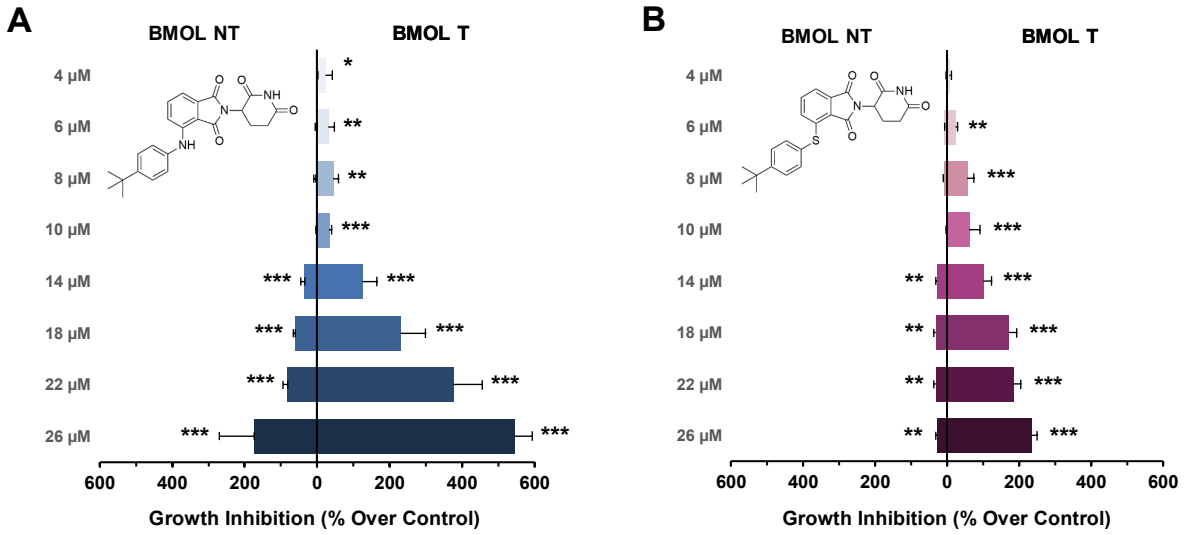

Figure 4: Effect of dose of lead compounds **6f** (A) and **7f** (B) on BMOL-NT and BMOL-T growth. Values reported as mean % change in doubling time over control (n = 3 in all cases), error bars represent SEM. * = $p < 0.05$, ** = $p < 0.01$, *** = $p < 0.001$.

The modern paradigm surrounding CELMoDs and their derivatives implies that their pleiotropic actions stem from the recruitment and ubiquitination of unique protein neosubstrates to the CRL4-CRBN complex; we inferred that our related compounds might also elicit their HCC anticancer actions through this same mode of action. It has previously been shown that methylation of a CELMoD 's glutarimide nitrogen abrogates cereblon binding, thus reducing induced protein degradation (Figure 5).[13,47,50,51]

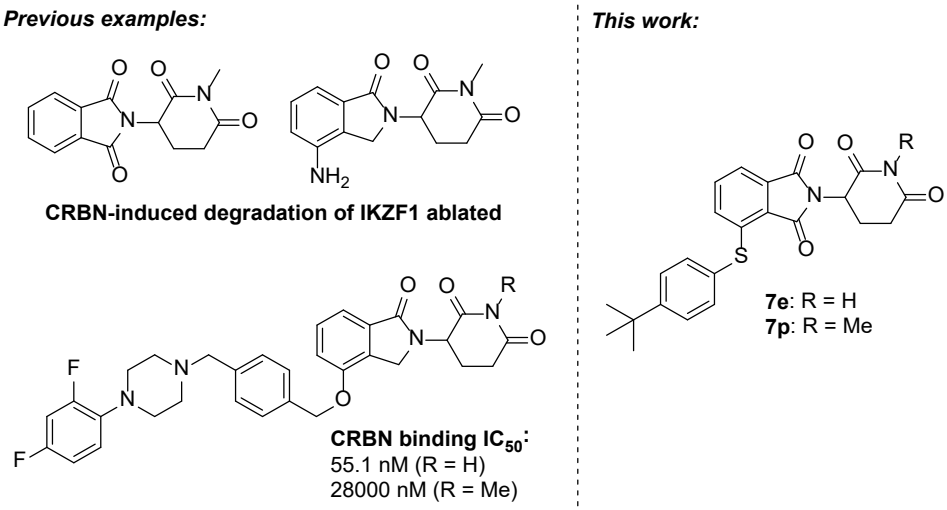

Figure 5: Examples from the literature of *N*-methylation at glutarimide as a method of inhibiting CRBN binding, and the structure of our *N*-methyl derivative **7p**.[47,51]

We therefore investigated the effect of N-methylation of our most potent selective derivative **7e** (Table 3). This comparatively small structural modification had a dramatic effect on both

cell proliferation inhibition potency and selectivity; decreasing activity against tumorigenic cells by 73%, while also causing significant inhibition of the non-tumorigenic line that was not previously observed. Methylation appeared to invert selectivity, from a strong (26-fold) preference for inhibition of BMOL-T growth, to a 2-fold preference for the non-tumorigenic line. This would strongly suggest that the imide proton is an essential motif for selective anticancer activity, presumably serving as a key hydrogen bond donor during binding. These data provide initial evidence supporting the hypothesis that our new thalidomide derivatives share CRBN as a binding target with the rest of the CELMoD class of drugs.

Table 3: Effect of *N*-methylation on activity and selectivity of compound **7e** against BMOL cell growth. Growth is reported as mean doubling times in hours *(n* = 3 in all cases, with SEM in parentheses), control represents 0.1% DMSO vehicle in supplemented growth medium. Statistical significance is indicated as follows: * = $p < 0.05$, ** = $p < 0.01$, *** = $p < 0.001$.

Compd.	**BMOL-NT**			**BMOL-T**		
	Growth *(SEM)*	% Change	*p*	Growth *(SEM)*	% Change	*p*
Control	19.0 *(0.5)*	**-**	-	14.3 *(0.1)*	**-**	-
7e	19.3 *(0.6)*	**+2%**	NS	20.1 *(2.4)*	**+51%**	***
7p	24 *(2.5)*	**+26%**	**	16.3 *(0.2)*	**+14%**	*

When considering the potential role of CBRN as a target for the resulting pharmacology of our compounds, it should be noted that despite high residue conservation between species, CELMoD binding to rodent CRBN does not induce the degradation of IKZF1/3 or CK1α seen in humans.[52] Mutation studies have identified a single variant residue in the ligand binding domain of CRBN responsible for this insensitivity; human valine 387 is replaced with isoleucine in the matching position for rodent CRBN (residue 390).[53] To better understand the role of this residue, we performed three replicate MD simulations with each of thalidomide, 6f and 7f in the binding site. Thalidomide site centrally in the binding pocket formed by multiple tryptophan residues as seen in Fig 5A, with two hydrogen bonds between the glutarimide ring and the protein backbone as seen in the crystal structure. The long side chains of 6f and 7f, however, allow for a range of additional interactions with the protein shown in Fig 5A. To better quantify these, we determine the average interaction energy between the ligand each protein residue across the duration of 3 replicate 100ns simulations as shown in Fig 5B. This shows that all compounds have the strongest association with W382, W388, W402 as well as additional interactions with H380 and H399. Interestingly, 6f is seen to be relatively mobile, with the side chain interchanging between three primary conformations pointing toward either H380, W382 or H399. Despite having bulky sidechains, 6f and 7f have only slightly greater interactions with the protein than the parent compound.

While I390 does not have significant interactions with any of the simulated compounds, it does sit directly beside them and is particularly close to the sidechain of 7f. It is proposed that the added bulk of the introduced isobutyl sidechain in rodent versus human CBRN precludes substrate interactions with either the CELMoD amino group or other residues peripheral to the binding pocket. The strong response in murine liver cells elicited by our derivatives is therefore especially interesting, as it leaves no role for any known CELMoD neosubstrates such as IKZF1, IKZF3, CK1α, ZFP91 in their mechanism of action. Moreover, it would suggest that either CRBN binding plays no role in their activity and involves

altogether different mode of action, or that the neosubstrate(s) recruited by our derivatives to CRBN are unique,[ref] and require different interactions between protein, ligand and substrate.

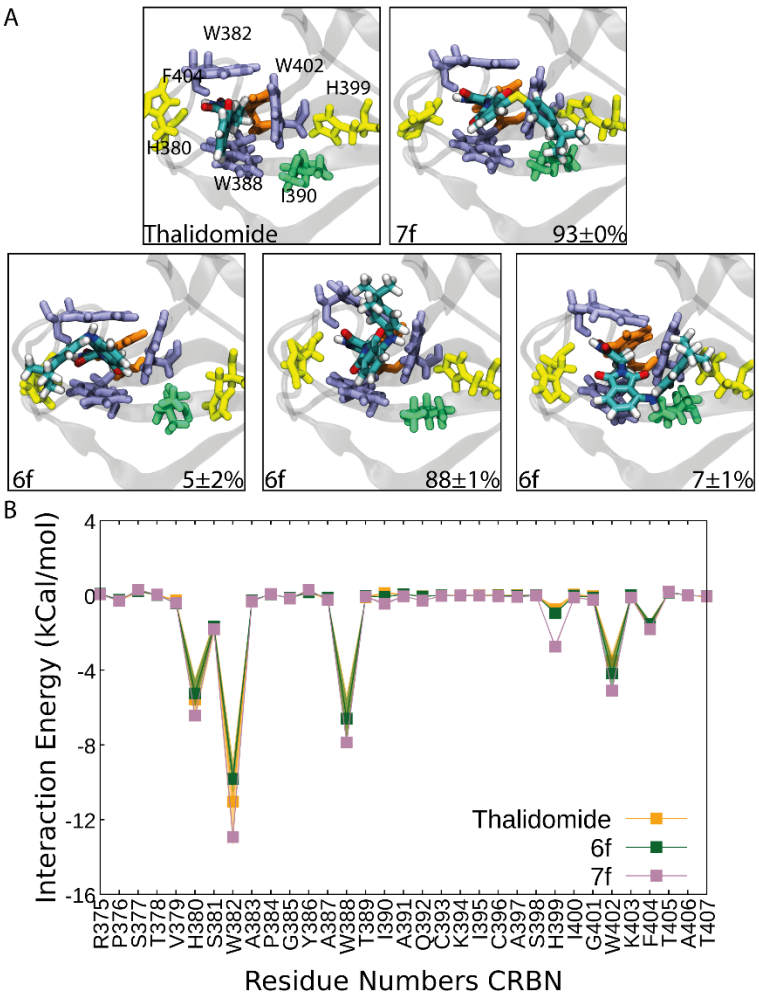

Figure 5: Binding poses of Thalidomide, 6f and 7f to murine CBRN from MD simulations. (A) Representative snapshots of the most likely binding pose of each compound is shown as found from replicate 100ns simulations. Residues are coloured by amino acid type while ligands are coloured by atom name. Three commonly occupied poses of 6f are shown. The protruding *sec*-butyl sidechain of isoleucine 391 is highlighted in green. (B) Average interaction energy between each compound and each protein residue highlighting the most significant residues for ligand binding. Shaded regions show the standard deviation across the three replicate simulations.

Cell Migration Assays. The anti-angiogenic effect of CELMoDs has previously been attributed to halting of cell motility *via* inhibiting phosphorylation of targets including STAT3 and Akt. As these pathways have also been highlighted in the migration and invasion of HCC, we proposed that our compounds might possess anti-migratory effects in our unique tumorigenic liver progenitor cells. We therefore conducted a series of wound healing assays in

the BMOL-T line with the Incucyte Zoom live cell imaging system to investigate any influence on cancer cell migration (Figure 6). Remarkably, compounds **6f** and **7f** produced a pronounced and sustained inhibition of BMOL-T cell motility over a 24-hour period. In both cases, cell migration appeared to halt completely by 16 h, displaying mean reductions in wound closure of 94% (**6f**) and 80% (**7f**) over control respectively. In comparison, treatment with lenalidomide inhibited migration by just 20% at the equivalent dose (10 µM), and statistical analyses of the wound closure rate of each treatment failed to find a significant difference over control in the lenalidomide treatment. The discovery of anti-migratory properties in our derivatives is especially important when considering that the liver is the most common site of metastatic burden – fibrosis and myeloid cell accumulation often facilitate seeding and development of invasive tumour cells, which in HCC may promote intrahepatic metastasis.[54,55] Moreover, the development of extrahepatic metastatic disease as a complication of HCC would contraindicate surgical intervention, and so drug candidates demonstrating potentially anti-metastatic effects such as ours are especially promising.

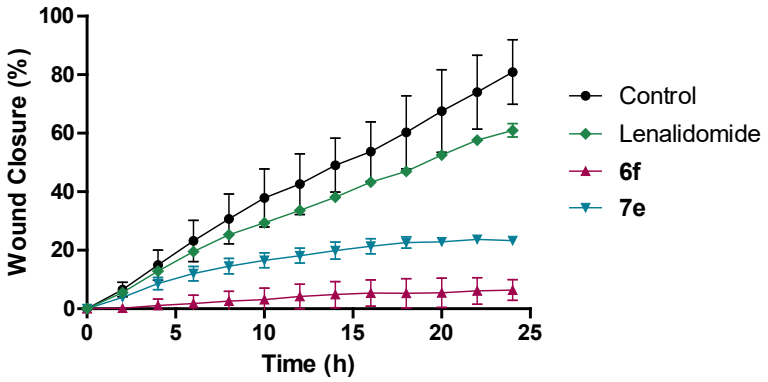

Figure 6: Effect of compound treatment on BMOL-T migration and wound healing assay. (*n* = 3 in all cases), error bars represent SEM. DMSO vehicle (0.1% in supplemented growth medium) served as a control. For associated statistical analyses of these data, see supporting information.

Cell signalling: quantifying levels and cellular localisation of phosphoproteins. Having identified novel thalidomide derivatives with antiproliferative and anti-migratory effects in tumorigenic liver cells, we sought to identify affected signalling pathways that might be involved in the respective cellular activities. Pathways that are known to be important in HCC development, growth, and/or invasion were prioritised, especially where these pathways had formally been implicated as a target of CELMoD therapy in other malignant cell lines. Based on these criteria the PI3k/Akt/mTOR, IL-6/JAK/STAT3, Ras/Raf/Mek/Erk and canonical NFκB (p65) signalling axes were selected for further study.[56–59] As a rapid preliminary screen, both BMOL lines were subjected to immunofluorescence assays of key downstream markers of these pathways using the CellInsight CX7 high-content screening platform (ThermoFisher). Individual fluorescence values per cell were measured, offering mean values representative of very large technical replicates (*n* = 1400 – 4500, depending on cell line) within each experiment. Furthermore, the ratio of signal originating from the nucleus vs. the mean whole-cell total was calculated based upon cross-staining of the nucleus, serving as a measure of treatment influence on nuclear localisation of a target protein. Additionally, the percentage of a cell population positive for the target protein is also quantified using this technique.

BMOL cells treated with either DMSO vehicle, lenalidomide, or target compounds **6f** and **7f** were subjected to immunofluorescent assays of the phosphorylated forms of canonical NFκB (p65), Akt, STAT3 and Erk (Table 4). Unsurprisingly, in our murine model lenalidomide was mostly ineffective in influencing protein levels or their nuclear localisation. No compound tested consistently affected the total cellular levels of p-Akt, but nuclear p-Akt was supressed by lenalidomide and **7f**. In this pathway thioether **7f** was slightly more potent than lenalidomide but displayed no selectivity between cell lines. All three test compounds were able to selectively reduce total levels of the phosphorylated form of NFκB (p65) preferentially in tumorigenic cells, in the following order of potency: **7f** > **6f** > lenalidomide. Compound **7f** also reduced mean nuclear localisation of p65 by 23%, suggesting a concomitant reduction of downstream transcription events in the canonical NFκB pathway. A similar profile of activity was observed in the immunofluorescence assay of p-STAT3, where lenalidomide and **6f** produced mild and inconsistent inhibition. Again, **7f** achieved significant selective suppression of both phosphorylated STAT3 levels, and their nuclear localisation. Many of STAT3's target genes have pro-oncogenic roles are implicated in tumour cell proliferation, survival and invasiveness.[59] Furthermore, STAT3 also inhibits the related STAT1 transcription factor which possesses tumour suppressive, pro-apoptotic effects.[60] Inhibition of STAT3 therefore is a prime mechanistic candidate that accounts for the actions of both thalidomide derivateves **6f** and **7f** in liver progenitor cells.

Table 4: Summary of immunofluorescent assays of BMOL cells screening for changes to phosphorylated NFκB (p65), Akt, and STAT3. Values represent the mean of two individual experiments alongside standard deviation in parentheses. DMSO vehicle (0.1% in supplemented growth medium) served as a control. Results deemed indicative of selective activity in tumourigenic cells are highlighted in bold.

pNFκB (p65)	Mean Intensity % Change *(SD)*	Mean Ratio (nuclear:total) % Change *(SD)*
BMOL-NT		
Control	-	-
Lenalidomide	+13% *(14.8)*	-9% *(2.1)*
6f	-1% *(8.5)*	-11% *(1.4)*
7f	0% *(5.7)*	+11 *(15.5)*
BMOL-T		
Control	-	-
Lenalidomide	-5% *(3.5)*	+7% *(14.3)*
6f	-7% *(9.9)*	-9% *(8.0)*
7f	**-13% *(0.7)***	**-23% *(3.2)***

pAkt	Mean Intensity % Change *(SD)*	Mean Ratio (nuclear:total) % Change *(SD)*
BMOL-NT		
Control	-	-
Lenalidomide	+10% *(4.9)*	-6% *(1.9)*
6f	+4% *(0.7)*	-10% *(4.1)*
7f	0% *(7.0)*	-25% *(4.7)*
BMOL-T		
Control	-	-
Lenalidomide	-9% *(10.6)*	-16% *(2.5)*
6f	+4% *(16.3)*	+4% *(27.4)*

7f	-3% *(25.5)*	-19% *(1.2)*

pSTAT3	Mean Intensity (% Change)	Mean Ratio (nuclear:total) % Change *(SD)*
BMOL-NT		
Control	-	-
Lenalidomide	+2% *(3.5)*	-3% *(11.2)*
6f	-4% *(0.7)*	-13% *(4.5)*
7f	-5% *(2.1)*	-8% *(11.8)*
BMOL-T		
Control	-	-
Lenalidomide	-4% *(3.5)*	+3% *(22.6)*
6f	-7% (*12.0)*	-10% *(7.5)*
7f	**-22% *(8.5)***	**-16% *(15.6)***

Cell signalling: quantifying expression and phosphorylation of STAT3 by AlphaLISA assay.

A more rigorous approach to confirm the involvement of the STAT3 pathway is to determine levels of both total STAT3 and pSTAT (canonical phosphorylation at Y705) in BMOL-T cells (Figure 6). Along with the three previous test compounds **6f**, **7f** and lenalidomide, *N*-methyl derivative **7p** was also included to ascertain whether loss of the glutarimide H-bond donor in **7f** would have the same ablative effect on STAT3 inhibition as it did on BMOL-T growth inhibition previously. Lenalidomide failed to significantly affect mean total STAT3, or STAT3 phosphorylation in this assay. While all three novel derivatives **6f**, **7f** and **7p** demonstrated lower mean values in STAT3 levels across triplicate experiments, inter-experimental variation of cell responses was particularly high, and no compound produced statistically significant changes to total STAT3 levels in BMOL-T cells, implying no influence on STAT3 expression in BMOL-T cells. Thioether **6e** alone significantly inhibited STAT3 phosphorylation (23% reduction over the control). Since *N*-methyl analogue **7p** did not share this activity it can be inferred the glutarimide proton is essential for both growth inhibition and downregulating STAT3 activation. Interestingly, despite the close structural resemblance and similar profiles of growth inhibition, we were not able to detect any significant effect on STAT3 signalling through the alphaLISA method. These results suggest that the nitrogen and sulfur-containing analogues presented in this study may operate through distinct mechanisms of action, despite their structural similarities. In the case of **7f** however, these data provide strong evidence implicating a role for the IL-6/JAK/STAT3 signalling axis in the biological activity of this compound in liver cancer.

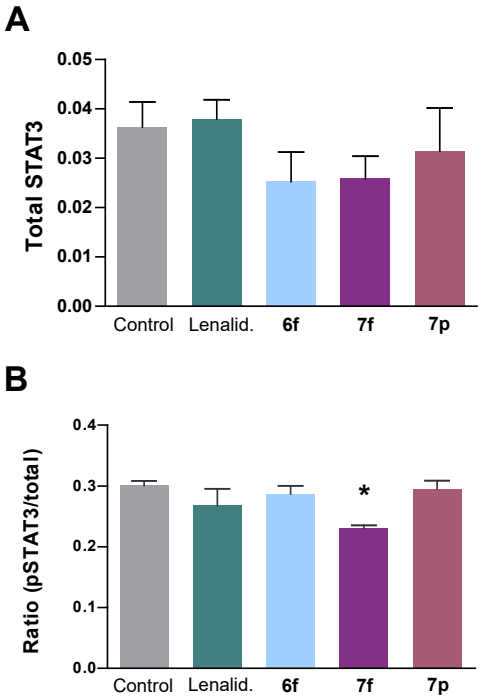

Figure 6: A) AlphaLISA assay measuring total cellular STAT3 in BMOL-T cells upon treatment with various agents at 10 µM. Values represent mean normalised fluorescence intensity (arbitrary units), error bars represent SEM ($n \geq 3$ in all cases). B) AlphaLISA assay measuring ratio of total cellular STAT3 to p-STAT3 in BMOL-T cells upon treatment with various agents at 10 µM. Values represent mean normalised fluorescence intensity, error bars represent SEM ($n \geq 3$ in all cases). * = $p < 0.05$, ** = $p < 0.01$, *** = $p < 0.001$. DMSO vehicle (0.1% in supplemented growth medium) served as a control.

Conclusion.

Growth assays in our unique cell lines revealed several novel thalidomide analogues that demonstrate selective antiproliferative activity in only tumourigenic cells. Most analogues assessed were also well tolerated by non-tumourigenic cells, and several demonstrated comparable or improved selective antiproliferative activity over our previously reported derivative **5b**. Benzyl and aryl sulfide-linked analogues of **5b** (**5f** and **5j**) retained selectivity and potency, while the equivalent ether (**5h**) was inactive. Generally, short branched alkyl substituents in the *para* position performed best, while derivatives bearing alkyl thioether motifs or N-heterocyclic substituents all performed poorly in growth assays. Two *tert*-butyl substituted derivates (aryl amine **6f** and aryl sulfide **7f**) were the most promising compounds assessed, demonstrating selective inhibition of only BMOL-T cells at 10 µM (31% and 36% respectively). Both compounds also exhibited remarkable anti-migratory activity, eliciting 94% (**6f**) and 80% (**7f**) inhibition of BMOL-T cell motility at this dose during wound healing assays. Furthermore, preliminary analyses of key signal pathways revealed **7f** inhibits STAT3 phosphorylation and selectively downregulates nuclear localisation of pSTAT3 in BMOL cells. In summary, this work has highlighted that modifications to the thalidomide core structure can yield derivatives with promise as selective anticancer agents against HCC, and that further study is warranted into their development as potential therapeutics.

Experimental:

Cell Maintenance. BMOL-NT and BMOL-T cells were maintained as previously described by Woo *et al*. in 25 cm^2 flasks (Corning), with 3 mL of Williams' E Medium (WEM) supplemented with; 675 µg/mL Streptomycin (Life Technologies), 1% v/v Fungizone (Life Technologies), 48.4 µg/mL Penicillin (Calbiochem), 20 ng/mL EGF (Corning), 30 ng/mL IGF-II (GroPrep Bioreagents), 0.25 U/mL Humulin R (Eli Lilly and Company), 2 mM Glutamine (Sigma-Aldrich) and 5% Fetal Bovine Serum (FBS, Life Technologies). Medium was replaced every 2 days (3 days over the weekend with an additional 2 mL of medium). Once cells reached approximately 70% confluence they were passaged into new flasks. Cells were detached by rinsing with 1 mL of Hank's Balanced Salt Solution (HBSS, Sigma-Aldrich), then 1 mL of 0.05% Trypsin (Life Technologies) in HBSS, followed by a 5 min incubation at 37 ºC. After cells had rounded and detached, they were resuspended in 1 mL of medium and passaged as required.

Growth Assay Protocol. Proliferation assays were performed as follows, modified from a procedure described by Woo *et al.* BMOL cells (BMOL-T: 1000 per well, BMOL-NT: 1500 per well) were plated into 96-well plates (Greiner Bio-One) in 100 µL supplemented medium per well, and left to attach in the Incucyte instrument overnight. The following day an additional 100 µL of medium was added (either vehicle or containing a compound treatment as required; see below) and each plate was imaged every four hours for three days. Compound treatments were performed in six replicate wells per cell type, for a total of 12 wells per treatment. The Incucyte instrument's cell detection algorithm was trained on a set of 20 representative images from both cell lines at a range of confluence levels. The efficiency of cell detection was checked manually by visual examination to ensure only cells were detected. The log of cell confluency (measured as % well coverage) was plotted against time to generate a growth curve. The doubling time was determined from the linear portion of each curve corresponding to the log (exponential) phase of cell growth.

Treatment of Cells with Thalidomide Derivatives. Solutions of all tested compounds were prepared at 2x (20 µM) concentrations, with 0.2% DMSO in supplemented medium. Cells were treated with each compound by addition of 100 µL of these solutions, thereby achieving a final concentration of 1x and 0.1% DMSO in a final well volume of 200 µL.

Quantification and localisation of cell signalling proteins. Briefly, BMOL cells were cultured in Williams' essential medium (supplemented as described above) in 96-well plates and treated with indicated compounds from Table 4 or 0.1% DMSO vehicle in supplemented medium for 6 hours. Cells were washed with PBS lx, and affixed to plate using 4% PFA in phosphate buffered saline for 10 minutes; washed IX and permeabilized using 0.1% Triton-X-100 in PBS for 8 minutes; washed Ix and blocked with protein blocker (Cat.# xx) for 30 minutes. Cells were then incubated with the following primary antibodies: anti-phos-p65, anti-phos-Akt, anti-phos-STAT3, (diluted in DAKO diluent as per manufacturer's recommendations) for 18 hours. Cells were washed 3x prior to adding secondary antibodies and incubated for l hr, wash again, incubated with Hoescht reagent for 8 minutes. Cells were washed 2x and imaged/analyzed using the CX7 instrument with the HCS studio software package.

Cell Migration Assays. BMOL-T cells (20,000 cells per well) were plated in 96-well plates (Greiner Bio-One) in 100 µL supplemented medium per well, and incubated for 24 h. Wounds were made in wells using the Woundmaker™ device, then medium was aspirated and replaced with fresh supplemented medium (100 µL per well; either untreated, DMSO vehicle, or containing compound treats as required). The plate was placed in an IncucyteZOOM system and imaged every 2h for 24 h. Images were processed with the Incucyte software to obtain measurements of average wound width in micrometres, which were further processed using the Graphpad Prism 5 software package.

Statistical Analysis. Where appropriate, statistical significance was determined *via* one-way analysis of variance (ANOVA) with Dunnett's test post-hoc analysis, using the Graphpad Prism 5 software package. *p* values below 0.05 were considered statistically significant.

Chemistry. General Experimental

Starting materials and reagents were available from Merck, Sigma-Aldrich, Alfa Aesar, TCI, Precious Metals Online, Fluorochem, Oakwood Chemical, Fluka, Boron Molecular, and used without further purification unless otherwise stated. The $Pd_2(dba)_3$.$CHCl_3$ used in this work was synthesised according to literature procedures.[ref] Compounds **5a-d**, **6a-f**, **6i-j**, and **6n-o** were synthesized as previously described.[36] The abbreviated ligand name XPhos refers to 2-Dicyclohexylphosphino-2′,4′,6′-triisopropylbiphenyl, and XantPhos likewise refers to 4,5-Bis(diphenylphosphino)-9,9-dimethylxanthene. Anhydrous solvents were distilled over the appropriate drying agents according to Amarego and Chai, acquired from a Pure Solv 5-Mid Solvent Purification System (Innovative Technology Inc.) and degassed (argon) prior to use. Hexanes and ethyl acetate for chromatography were distilled prior to use. ^{1}H, ^{13}C, and ^{19}F Nuclear Magnetic Resonance (NMR) spectra were acquired on a Varian 300, Varian 400, Bruker AV500 or Bruker V600 spectrometer at 25 ºC. All signals δ are reported in parts per million (ppm). Chemical shifts in ^{1}H and ^{13}C spectra were referenced to the residual (partially) non-deuterated solvent according to Fulmer *et al.*[61] ^{19}F chemical shifts were referenced to the external standard hexafluorobeznene (-164.9 ppm). Wherever compound solubility allowed, $CDCl_3$ was used to acquire spectra preferentially over DMSO-d_6. Mass spectra were recorded on a Waters LCT Premier XE instrument (time-of-flight, electrospray ionisation in positive mode). Infrared spectra were acquired on a Perkin Elmer Spectrum One spectrometer at 2 cm^{-1} resolution equipped with an ATR diamond. The reported retention factors (Rf) were acquired via thin layer chromatography (TLC) performed on Merck silica gel 60 F254 pre-coated aluminium sheets. Column chromatography was performed using Davisil® chromatographic silica gel (40 – 63 micron) supplied by Adelab. Preparative thin layer chromatography (PTLC) was performed with in-house prepared plates (20 x 20 x 0.1 cm) using silica gel 60 PF254 containing gypsum supplied by Merck. The visualization of the developed plates was achieved using a 254-nm or 365-nm UV lamp.

General Procedure for Buchwald-Hartwig Amination Reactions.

To a flame-dried Schlenk flask was added the following in sequence, under an inert atmosphere of argon: 4-iodothalidomide (200 mg, 0.52 mmol), XPhos (40 mg, 0.083 mmol) $Pd_2(dba)_3{\cdot}CHCl_3$ (22 mg, 0.021 mmol) K_2CO_3 (144 mg, 1.04 mmol) 1,4-dioxane (2 mL) and

The desired aniline (0.89 mmol). The reaction mixture was stirred at 90 °C for 18 h and the resulting mixture then cooled to room temperature, diluted with ethyl acetate (10 mL) and filtered through a pad of celite. The filter cake was washed with ethyl acetate (*ca.* 40 mL) and the resulting filtrate adsorbed to silica. Purification by flash column chromatography (ethyl acetate/hexanes) gave the desired aminated thalidomide analogue.

2-(2,6-Dioxopiperidin-3-yl)-4-[(4-butylphenyl)amino]isoindole-1,3-dione (6g). Following the general procedure for Buchwald-Hartwig amination reactions, using 4-butylaniline (123 mg, 0.79 mmol) the title compound was obtained after purification by flash column chromatography (30% → 50% ethyl acetate/hexanes) as a yellow solid (207 mg, 98%). **R_f =** 0.33 (40% ethyl acetate/hexane); **mp** = 205–207 °C; ^{1}H **NMR** (500 MHz, DMSO-d_6) δ 11.13 (s, 1H), 8.33 (s, 1H), 7.58 (dd, J = 8.6, 7.1 Hz, 1H), 7.34 (d, J = 8.5 Hz, 1H), 7.21 (dd, J = 8.0, 5.3 Hz, 5H), 5.12 (dd, J = 12.9 & 5.4 Hz, 1H), 2.90 (ddd, J = 17.3, 14.0 & 5.4 Hz, 1H), 2.66 – 2.52 (m, 4H), 2.14 – 1.98 (m, 1H), 1.56 (quint., J = 7.4 Hz, 2H), 1.32 (sext., J = 7.4 Hz, 2H), 0.90 (t, J = 7.4 Hz, 3H); **^{13}C NMR** (126 MHz, DMSO) δ 173.2, 170.5, 168.8, 167.5, 143.8, 138.9, 137.3, 136.6, 132.9, 129.7, 122.9, 119.4, 113.4, 111.8, 49.1, 34.7, 33.6, 31.4, 22.6, 22.2, 14.2; **IR** (neat) 3324 (N-H) 3205 (N-H), 1757 (C=O), 1689 (C=O), 1619 (C=O), 1401, 1320 cm^{-1}; **HRMS** calculated for $C_{23}H_{24}N_3O_4$: 406.1767, found: 406.1770 $[M+H]^+$.

2-(2,6-Dioxopiperidin-3-yl)-4-(5,6,7,8-tetrahydronaphthalen-2-ylamino)isoindole-1,3-dione (6h). Following the general procedure for Buchwald-Hartwig amination reactions, using the coupling partner 5,6,7,8-tetrahydro-2-naphthylamine (60 mg, 0.41 mmol), the title compound was obtained after purification by flash column chromatography (20% → 50% ethyl acetate/hexanes) as a yellow solid (76 mg, 72%). **R_f** = 0.53 (40% ethyl acetate/hexanes); **mp** = 208 –210 °C; **^{1}H NMR** (400 MHz, DMSO-d_6) δ 11.12 (s, 1H), 8.26 (s, 1H), 7.58 (dd, J = 8.6, 7.1 Hz, 1H), 7.34 (d, J = 8.5 Hz, 1H), 7.20 (dd, J = 7.1, 0.6 Hz, 1H), 7.10 – 6.98 (m, 2H), 5.11 (dd, J = 12.9, 5.4 Hz, 1H), 2.90 (ddd, J = 17.2, 14.0, 5.4 Hz, 1H), 2.71 (d, J = 4.0 Hz, 4H), 2.66 – 2.52 (m, 2H), 2.08 – 2.02 (m, 1H), 1.74 (quint., J = 3.0 Hz, 4H); **^{13}C NMR** (101 MHz, DMSO-d_6) δ 172.8, 170.0, 168.4, 167.09, 143.5, 137.8, 136.4, 136.2, 132.9, 132.4, 129.8, 122.8, 120.0, 119.1, 112.9, 111.2, 48.7, 31.0, 28.8, 28.3, 22.8, 22.6, 22.1; **IR** (neat) 3355 (N-H), 3239 (N-H), 3103, 1761 (C=O), 1690 (C=O), 1620 (C=O), 1604 (C=O), 1476, 1403, 1321 cm^{-1}; **HRMS** calculated for $C_{23}H_{22}N_3O_4$: 404.1610, found: 404.1615 $[M+H]^+$.

2-(2,6-Dioxopiperidin-3-yl)-4-[(4-isopropoxyphenyl)amino]isoindole-1,3-dione (6k). Following the general procedure for Buchwald-Hartwig amination reactions, using the coupling partner 4-isopropoxyaniline (52 mg, 0.24 mmol), the title compound was obtained after purification by flash column chromatography (40% ethyl acetate/hexane) as an orange solid (35 mg, 54%). **R_f** = 0.36 (40% ethyl acetate/hexane); **mp** = 212–214 °C; **^{1}H NMR** (400 MHz, DMSO-d_6) δ 11.12 (s, 1H), 8.22 (s, 1H), 7.55 (dd, J = 8.5, 7.2 Hz, 1H), 7.30 – 7.12 (m, 4H), 6.96 (d, J = 8.9 Hz, 2H), 5.11 (dd, J = 12.9 & 5.4 Hz, 1H), 4.60 (hept, J = 6.4 Hz, 1H), 2.90 (ddd, J = 18.0, 13.8 & 5.5 Hz, 1H), 2.66 – 2.53 (m, 2H), 1.99-2.07 (m, 1H), 1.27 (d, J = 6.0 Hz, 6H); **^{13}C NMR** (101 MHz, DMSO-d_6) δ 173.3, 170.5, 168.9, 167.6, 155.2, 144.7, 136.6, 132.8, 132.0, 125.8, 119.0, 116.9, 112.9, 111.1, 69.9, 49.1, 31.4, 22.6, 22.3; **IR** (neat) 3320 (N-H), 3229 (N-H), 1759 (C=O), 1621 (C=O), 1510, 743 cm^{-1}; **HRMS** calculated for $C_{22}H_{22}N_3O_5$: 408.1559, found: 408.1554 $[M+H]^+$.

2-(2,6-Dioxopiperidin-3-yl)-4-{[4-(dimethylamino)phenyl]amino}isoindole-1,3-dione (6l). Following the general procedure for Buchwald-Hartwig amination reactions, using *N,N*-dimethyl-*p*-phenylenediamine (120 mg, 0.89 mmol), the title compound was obtained after purification by flash column chromatography (50% ethyl acetate/hexanes) as a brown solid (35 mg, 15%). $\mathbf{R_f}$ = 0.21 (50% ethyl acetate/hexanes); **^{1}H NMR** (400 MHz, DMSO-d_6) δ 11.11 (s, 1H), 8.10 (s, 1H), 7.62 – 7.39 (m, 1H), 7.22 – 6.96 (m, 3H), 6.78 (d, J = 9.0 Hz, 1H), 5.10 (dd, J = 12.9 & 5.4 Hz, 1H), 2.91 (s, 6H), 2.64 – 2.53 (m, 2H), 2.10 – 2.02 (m, 1H); **^{13}C NMR** (101 MHz, DMSO-d_6) δ 173.3, 170.5, 169.0, 167.6, 148.9, 145.5, 136.5, 132.8, 128.1, 125.9, 118.8, 113.6, 112.4, 110.5, 49.1, 31.4, 22.6; **IR** (neat) 3362 (N-H), 3264 (N-H), 1760 (C=O), 1732 (C=O), 1683 (C=O), 1622 (C=O), 1522 cm^{-1}; **HRMS** calculated for $C_{21}H_{21}N_4O_4$: 393.1563, found: 393.1574 $[M+H]^+$.

2-(2,6-Dioxopiperidin-3-yl)-4-{[4-(trifluoromethyl)phenyl]amino}isoindole-1,3-dione (6m). Following the general procedure for Buchwald-Hartwig amination reactions, 4-trifluoromethylaniline (64 mg, 0.39 mmol) was coupled with 4-iodothalidomide (99 mg, 0.26 mmol). Purification by flash column chromatography (40% ethyl acetate/hexanes) afforded the desired compound (60 mg, 67%) as a yellow solid. $\mathbf{R_f}$ = 0.36 (40% ethyl acetate/hexanes); **mp** = 259–261 °C; **^{1}H NMR** (400 MHz, DMSO-d_6) δ 11.13 (s, 1H), 8.88 (s, 1H), 7.76 – 7.61 (m, 4H), 7.43 (dd, J = 24.6, 7.4 Hz, 3H), 5.13 (dd, J = 12.9, 5.4 Hz, 1H·), 2.97 – 2.82 (m, 1H), 2.70 – 2.55 (m, 1H), 2.18 – 2.02 (m, 1H); **^{13}C NMR** (101 MHz, DMSO-d_6) δ 172.8, 170.0, 167.6, 166.9, 144.3, 140.7, 136.2, 132.7, 126.5 (q, J = 3.8 Hz), 125.9, 123.2, 122.5, 122.2, 122.0, 119.3, 115.3, 114.7, 48.8, 31.0, 22.1; **^{19}F NMR** (376 MHz, DMSO-d_6) δ -57.89; **IR** (neat) 3316 (N-H), 3210 (N-H), 1765 (C=O), 1695 (C=O), 1319, 1112, 741 cm^{-1}; **HRMS** calculated for $C_{20}H_{15}N_3O_4F$: 418.1015, found: 418.1017 $[M+H]^+$.

4-benzyl-2-(2,6-dioxopiperidin-3-yl)isoindoline-1,3-dione (5e). To a flame-dried reaction vial, 4-iodothalidomide (100 mg, 0.26 mol), $Pd_2(dba)_3{\cdot}CHCl_3$ (22 mg, 0.021 mmol), triphenylphosphine (68 mg, 0.26 mmol), Ag_2O (121 mg, 0.52 mmol) were added. The vial was evacuated and backfilled with argon three times, then fitted with a PTFE septum and THF (1.5 mL) was added, followed by benzyl boronic acid pinacol ester (87 µL, 0.39 mmol). The reaction vial was sealed under argon and heated to reflux for 18 h with stirring. After cooling to room temperature solvent was removed *in vacuo* and the residue was passed through a silica plug (20→50% ethyl acetate/hexanes), then purified by PTLC (50% ethyl acetate/hexanes) to afford the title compound as a white solid (61 mg, 67%). $\mathbf{R_f}$ = 0.48 (50% ethyl acetate/hexanes); **mp** = 195–197 °C; **^{1}H NMR** (500 MHz, $CDCl_3$) δ 8.04 (s, 1H), 7.74 (d, J = 7.3 Hz, 1H), 7.62 (t, J = 7.6 Hz, 1H), 7.47 (d, J = 7.8 Hz, 1H), 7.33 – 7.28 (m, 2H), 7.28 – 7.21 (m, 4H), 4.99 (dd, J = 12.4 & 5.4 Hz, 1H), 4.49 (s, 2H), 2.94 – 2.70 (m, 3H), 2.20 – 2.12 (m, 1H); **^{13}C NMR** (126 MHz, $CDCl_3$) δ 170.9, 168.1, 168.0, 167.3, 147.4, 142.1, 136.4, 136.4, 134.4, 132.3, 129.2, 128.1, 126.9, 122.0, 49.3, 36.3, 33.9, 31.5, 29.9, 25.0, 24.1, 22.8; **IR** (neat): 3216 (N-H), 3084, 1770 (C=O), 1700 (C=O), 1601, 1388, 1322, 1256, 1194, 1119, 737, 700 cm^{-1}; **HRMS** calculated for $C_{20}H_{17}N_2O_4$: 349.1188, found: 349.1189 $[M+H]^+$.

2-(2,6-Dioxopiperidin-3-yl)-4-(4-isopropylbenzyl)isoindoline-1,3-dione (5f). Prepared as described for **5e** above, using 4-iodothalidomide **4a** (50 mg, 0.18 mmol) and 4-isopropylbenzyl boronic acid pinacol ester (71 mg, 0.27 mmol). Purification of the crude residue by PTLC (25% ethyl acetate/hexanes, then redeveloped in 35% ethyl acetate/hexanes) afforded the desired product as a white solid (22 mg 41%). $\mathbf{R_f}$ = 0.42 (40% ethyl acetate/hexanes); **mp** 137-140 °C; **^{1}H NMR** (500 MHz, $CDCl_3$) δ 8.03 (s, 1H), 7.73 (dd, J = 7.3, 1.0 Hz, 1H), 7.62 (t, J = 7.6 Hz, 1H), 7.49 (dd, J = 7.8, 1.0 Hz, 1H), 7.20 – 7.15 (m, 4H), 4.99 (dd, J = 12.4, 5.4 Hz, 1H), 4.45 (s, 2H), 2.94 – 2.71 (m, 4H), 2.19 – 2.13 (m, 1H), 1.23 (d, J = 6.9 Hz, 6H); **^{13}C NMR** (126 MHz, $CDCl_3$) δ 170.9, 168.1, 168.0, 167.3, 147.4, 142.1, 136.4, 136.4, 134.4, 132.3, 129.2, 128.1, 126.9, 122.0, 49.3, 36.3, 33.9, 31.5, 29.9, 25.0, 24.1, 22.8; **IR** (neat) 3214 (N-H), 2959, 1771 (C=O), 1702 (C=O), 1616, 1512, 1389, 1258, 1193, 1117, 737 cm^{-1}; **HRMS** calculated for $C_{23}H_{23}N_2O_4$: 391.1658, found: 391.1657 $[M+H]^+$.

2-(2,6-Dioxopiperidin-3-yl)-4-phenoxyisoindoline-1,3-dione (5g). To a round-bottom flask fitted with a reflux condenser was added 3-fluorophthalic anhydride (355 mg, 2.2 mmol), phenol (190 mg, 2.42 mmol), and potassium fluoride (192 mg, 3.3 mmol) followed by DMF (2.0 mL), and the ensuing solution heated to reflux for 2 h. After cooling to room temperature, the mixture was poured over ice cold water (50 mL) and the resulting precipitate was collected by vacuum filtration. After drying under high vacuum, a white solid (155 mg) was obtained that was carried through to the subsequent step without further purification. To a flame-dried flask under an inert atmosphere of argon was added the crude 3-phenoxyphthalic anhydride (145 mg, 0.60 mmol), 3-aminopiperidine-2,6-dione trifluoroacetate (153 mg, 0.63 mmol), and sodium acetate (59 mg, 0.72 mmol). Glacial acetic acid was added (1.8 mL, 3 M) and the mixture was heated to reflux with stirring for 16 h. After cooling the reaction to room temperature, solvent was removed under reduced pressure and the residue was redissolved in ethyl acetate and cooled in an ice bath. The resulting precipitate was collected by vacuum filtration, washed three times with water and ethyl acetate, then dried under high vacuum to give the title compound as a white solid (202 mg, 28% over 2 steps). $\mathbf{R_f}$ = 0.37 (40% ethyl acetate/hexanes); **mp** = 244–246 °C; **^{1}H NMR** (500 MHz, DMSO-d_6) δ 11.12 (s, 1H), 7.84 – 7.76 (m, 1H), 7.64 (d, J = 7.2 Hz, 1H), 7.48 (t, J = 7.9 Hz, 2H), 7.28 (t, J = 7.4 Hz, 1H), 7.17 (dd, J = 12.8, 8.1 Hz, 3H), 5.13 (dd, J = 12.8, 5.4 Hz, 1H), 2.89 (ddd, J = 17.0, 14.0, 5.4 Hz, 1H), 2.65 – 2.53 (m, 2H), 2.10 – 2.01 (m, 1H); **^{13}C NMR** (126 MHz, DMSO) δ 172.8, 169.9, 166.6, 164.9, 154.8, 153.9, 137.2, 133.6, 130.5, 125.1, 123.6, 119.8, 118.5, 117.9, 31.0, 22.0; **IR** (neat) 3100 (N-H), 1775 (C=O), 1705 (C=O), 1610, 1588, 1475, 1394, 1256, 1201, 748 cm^{-1}; **HRMS** calculated: 351.0981, found: 351.0989 $[M+H]^+$.

2-(2,6-dioxopiperidin-3-yl)-4-(4-isopropylphenoxy)isoindoline-1,3-dione (5h). To a round-bottom flask fitted with a reflux condenser was added 3-fluorophthalic anhydride (332 mg, 2.0 mmol), potassium fluoride (232 mg, 4.0 mmol), 4-isopropylphenol (409 mg, 3.0 mmol), DMF (2.0 mL), and the mixture was heated to reflux and stirred for 2 h. After cooling to room temperature, the reaction mixture was diluted with ethyl acetate (20 mL) then washed with saturated LiCl solution (3 x 20 mL), Na_2CO_3 solution (20 mL), water (20mL), and brine (20 mL). The organic layer was dried ($MgSO_4$), filtered, and removal of solvent under reduced pressure gave an orange oil (539 mg) that was carried forward without further purification. To a flame-dried flask under an inert atmosphere of argon was added the crude 4-(4-

isopropylphenoxy)isobenzofuran-1,3-dione (187 mg, 0.66 mmol), 3-aminopiperidine-2,6-dione trifluoroacetate (160 mg, 0.66 mmol) and sodium acetate (65 mg, 0.66 mg, 1.0 mmol) and glacial acetic acid (2.5 mL). The mixture was heated to reflux with stirring for 16 h. Concentration under reduced pressure afforded a crude oil which was subjected to column chromatography (25 → 40% ethyl acetate/hexanes) to give the title compound as a white solid (68 mg, 25% over 2 steps). $\mathbf{R}_f$ = 0.47 (40% ethyl acetate/hexanes); **mp** = 232–233 °C; **^{1}H NMR** (600 MHz, $CDCl_3$) δ 8.23 (s, 1H), 7.57 (dd, J = 8.3 & 7.4 Hz, 1H), 7.53 (dd, J = 7.2 & 0.6 Hz, 1H), 7.27 (s, 1H), 7.07 – 7.01 (m, 3H), 5.00 (dd, J = 12.5 & 5.4 Hz, 1H), 2.97 – 2.72 (m, 4H), 2.19 – 2.11 (m, 1H), 1.26 (d, J = 6.9 Hz, 6H); **^{13}C NMR** (151 MHz, $CDCl_3$) δ 171.1, 168.2, 167.0, 165.4, 156.0, 152.4, 146.4, 136.3, 133.9, 128.2, 122.6, 120.6, 118.3, 117.5; **IR** (neat) 3320 (N-H), 3229 (N-H) 1769 (C=O), 1621 (C=O), 1510, 743 cm^{-1}; **HRMS** calculated: 393.1450, found: 393.1454 $[M+H]^+$.

General Procedure for the Synthesis of Thioether Derivatives.

To a flame-dried Schlenk flask was added the following in sequence under an inert atmosphere of argon: 4-iodothalidomide **4a** (200 mg, 0.52 mmol), $Pd_2(dba)_3{\cdot}CHCl_3$ (16 mg, 0.016 mmol) and XantPhos (16 mg, 0.032 mmol), 1,4-dioxane (2 mL), diisopropylethylamine (0.50 mL, 1.04 mmol) and the required thiol (0.57 mmol). The reaction mixture was heated to 90 °C with stirring for 16 h, cooled to room temperature and diluted with ethyl acetate (10 mL). The mixture was filtered through a pad of celite, washing with ethyl acetate and DCM (*ca.* 20 mL each). The filtrate was adsorbed to silica and purified *via* flash column chromatography on silica to furnish the desired sulfide-functionalised thalidomide derivative.

2-(2,6-Dioxopiperidin-3-yl)-4-(phenylsulfanyl)isoindole-1,3-dione (5i). Following the above general procedure using thiophenol (32 mg, 0.29 mmol), the title compound was obtained after purification *via* flash column chromatography (40% ethyl acetate/hexanes) as a pale yellow solid (89 mg, 94%). **mp** = 243–245 °C; **^{1}H NMR** (400 MHz, DMSO-d_6) δ 11.16 (s, 1H), 7.94 – 7.27 (m, 7H), 6.94 (dd, J = 1 Hz, 1H), 5.17 (dd, J = 12.8 & 5.4 Hz, 1H), 2.91 (ddd, J = 16.8, 13.7 & 5.4 Hz, 1H), 2.69 – 2.53 (m, 2H), 2.16 – 2.03 (m, 1H); **^{13}C NMR** (126 MHz, DMSO-d_6) δ 172.8, 169.9, 166.7, 166.5, 139.0, 135.5, 135.2, 132.4, 130.6, 130.5, 130.3, 128.1, 124.9, 119.8, 49.0, 31.0, 21.9; **IR** (neat) 3190, 1764 (C=O), 1701 (C=O), 1253, 1185, 743 cm^{-1}; **HRMS** calculated for $C_{19}H_{15}N_2O_4S$: 367.0753, found: 367.0762 $[M+H]^+$.

2-(2,6-Dioxopiperidin-3-yl)-4-[(4-isopropylphenyl)sulfanyl]isoindole-1,3-dione (5j). Following the general procedure for the synthesis of thioether derivatives, using the coupling partner 4-isopropylbenzenethiol (81 mg, 0.53 mmol) the title compound was obtained after purification *via* flash column chromatography (35% ethyl acetate/hexanes) as a pale yellow solid (194 mg, 91%). $\mathbf{R}_f$ = 0.50 (40% ethyl acetate/hexanes); **mp** = 238–240 °C; **^{1}H NMR** (400 MHz, $CDCl_3$) δ 8.08 (s, 1H), 7.60 – 7.47 (m, 3H), 7.43 (dd, J = 8.2, 7.3 Hz, 1H), 7.35 (d, J = 8.1 Hz, 2H), 6.95 (dd, J = 8.1, 0.9 Hz, 1H), 5.01 (dd, J = 12.2, 5.4 Hz, 1H), 3.06 – 2.66 (m, 4H), 2.26 – 2.08 (m, 1H), 1.30 (d, J = 6.9 Hz, 6H); **^{13}C NMR** (101 MHz, $CDCl_3$) δ 170.7, 167.9, 167.0, 166.8, 151.3, 141.8, 136.0, 134.2, 132.5, 131.0, 128.3, 125.2, 125.0, 119.5, 49.2, 34.0, 31.4, 23.8, 22.6; **IR** (neat) 3213 (N-H), 1770 (C=O), 1702 (C=O), 1602, 1390, 745 cm^{-1}; **HRMS** calculated for $C_{22}H_{21}N_2O_4S$: 409.1222, found: 409.1233 $[M+H]^+$.

2-(2,6-Dioxopiperidin-3-yl)-4-((4-isopropylphenyl)sulfonyl)isoindoline-1,3-dione (5k). A solution of 77% *meta*-chloroperbenzoic acid (134 g, 0.6 mmol) in dichloromethane (2 mL) was added dropwise to a stirred solution of sulfide derivative **5j** (85 mg, 0.21 mmol) in dichloromethane (2 mL). The resulting pale green solution was left to stir for 24 h, then treated with sodium thiosulfate (2 mL) followed by dichloromethane (6 mL). The mixture was extracted with sodium bicarbonate (3 x 10 mL), washed with brine (2 x 10 mL), dried ($MgSO_4$), filtered and solvent removed under reduced pressure. Purification by PTLC (DCM) afforded the desired sulfone **5k** as a white solid (53 mg, 58%). $\mathbf{R_f}$ = 0.63 (10% MeOH/DCM); **mp** = °C; **^{1}H NMR** (400 MHz, $CDCl_3$) δ 8.58 (dd, J = 7.9, 1.1 Hz, 1H, Ar-H), 8.13 – 8.02 (m, 4H), 7.96 (t, J = 7.7 Hz, 1H), 7.37 (d, J = 8.4 Hz, 2H), 4.96 (dd, J = 12.4 & 5.3 Hz, 1H), 3.02 – 2.61 (m, 4H), 2.19 – 2.09 (m, 1H), 1.24 (d, J = 6.9 Hz); **^{13}C NMR** (101 MHz, CD_2Cl_2) δ 170.9, 168.0, 166.1, 166.0, 156.6, 148.8, 137.6, 135.3, 134.0, 133.0, 128.5, 128.3, 125.1, 123.3, 50.1, 34.7, 31.7, 30.1, 23.67, 22.8; **IR** (neat) 3255 (N-H), 3090 (N-H), 1784 (C=O), 1706 (C=O), 1383, 1320 (S=O), 1160, 1122 (S=O) cm^{-1}; **HRMS** calculated for $C_{22}H_{21}N_2O_6S$: 441.1120, found: 441.1118 $[M+H]^+$.

2-(2,6-Dioxopiperidin-3-yl)-4-(pyrimidin-2-ylthio)isoindoline-1,3-dione (7a). Following the general procedure for the synthesis of thioether derivatives, using the coupling partner 2-mercaptopyrimidine (64 mg), the title compound was obtained after purification *via* flash column chromatography (40 → 70% ethyl acetate/hexanes) as a pale yellow solid (158 mg, 82%). $\mathbf{R_f}$ = 0.38 (70% ethyl acetate/hexanes); **mp** = 244–246 °C; **^{1}H NMR** (500 MHz, $CDCl_3$) δ 8.52 (d, J = 4.9 Hz, 2H), 8.05 – 7.99 (m, 2H), 7.95 (dd, J = 7.5 and 1.0 Hz, 1H), 7.79 (t, J = 7.7 Hz, 1H), 7.06 (t, J = 4.8 Hz, 1H), 4.95 (dd, J = 12.4 and 5.3 Hz, 1H), 2.89 (dt, J = 16.6 and 2.3 Hz, 1H), 2.84 – 2.69 (m, 2H), 2.16 – 2.10 (m, 1H);**^{13}C NMR** (126 MHz, $CDCl_3$) δ 170.8, 170.6, 167.7, 166.6, 165.8, 157.8, 140.7, 134.6, 133.5, 132.1, 130.1, 124.2, 118.0, 49.4, 31.5, 22.7; **IR** (neat) 3277 (N-H), 1767 (C+O), 1704 (C=O), 1552, 1381, 1178, 890, 744 cm^{-1}; **HRMS** calculated for $C_{17}H_{13}N_4O_4S$: 369.0658, found: 369.0658 $[M+H]^+$.

2-(2,6-dioxopiperidin-3-yl)-4-(quinolin-2-ylthio)isoindoline-1,3-dione (8b). Following the general procedure for the synthesis of thioether derivatives, using the coupling partner 2-quinolinethiol (93 mg), the title compound was obtained after purification *via* flash column chromatography (30 → 60% ethyl acetate/hexanes) as an orange solid (188 mg, 87%); $\mathbf{R_f}$ = 0.23 (40% ethyl acetate/hexanes); **^{1}H NMR** (500 MHz, $CDCl_3$) δ 8.12 (d, J = 8.5 Hz, 1H), 7.98 (s, 1H), 7.95 – 7.89 (m, 2H), 7.87 – 7.80 (m, 2H), 7.75 – 7.67 (m, 2H), 7.55 (ddd, J = 8.0, 6.9, 1.2 Hz, 1H), 7.46 (d, J = 8.5 Hz, 1H), 4.99 (dd, J = 12.4, 5.4 Hz, 1H), 2.95 – 2.70 (m, 3H), 2.21 – 2.12 (m, 1H); **^{13}C NMR** (151 MHz, $CDCl_3$) δ 170.8, 167.8, 166.8, 166.2, 155.8, 148.5, 137.8, 137.3, 134.4, 133.7, 133.1, 130.4, 129.7, 128.9, 127.8, 127.0, 126.9, 122.7, 122.7, 49.5, 31.5, 22.7; **IR** (neat): 3088, 1770 (C=O), 1703 (C=O), 1387, 1194, 739 cm^{-1}; **HRMS** calculated: 418.0862, found: 418.0865 $[M+H]^+$.

2-(2,6-Dioxopiperidin-3-yl)-4-(*o*-tolylthio)isoindoline-1,3-dione (7c). Following the above general procedure for the synthesis of thioether derivatives, using the coupling partner 2-methylbenzenethiol (71 mg, 0.57 mmol), the title compound was obtained after purification *via* flash column chromatography (20 → 40% ethyl acetate /hexanes) as an off-white solid (167 mg, 84%). $\mathbf{R_f}$ = 0.42 (40% ethyl acetate/hexanes); **mp** = 249–251 °C; **^{1}H NMR** (500 MHz,

$CDCl_3$) δ 8.28 (s, 1H), 7.59 (dd, J = 7.5, 1.4 Hz, 1H), 7.55 (dd, J = 7.3, 0.9 Hz, 1H), 7.45 – 7.39 (m, 3H), 7.30 (td, J = 7.4, 1.8 Hz, 1H), 6.75 (dd, J = 8.2, 0.8 Hz, 1H), 5.05 – 4.99 (m, 1H), 2.94 – 2.74 (m, 3H), 2.40 (s, 3H), 2.21 – 2.15 (m, 1H); **^{13}C NMR** (126 MHz, $CDCl_3$) δ 171.0, 168.1, 167.1, 167.0, 143.7, 140.8, 137.4, 134.5, 132.9, 131.5, 130.9, 130.5, 127.8, 127.7, 125.4, 119.7, 49.4, 31.5, 22.8, 20.9; **IR** (neat): 3185 (N-H), 2918, 1768 (C=O), 1731 (C=O), 1693 (C=O), 1603, 1459, 1388, 1207, 1013, 747 cm^{-1}; **HRMS** calculated for $C_{20}H_{17}N_2O_4S$: 381.0909, found: 381.0906 $[M+H]^+$.

2-(2,6-Dioxopiperidin-3-yl)-4-(*m*-tolylthio)isoindoline-1,3-dione (7d). Following the general procedure for the synthesis of thioether derivatives, using the coupling partner 3-methylbenzenethiol (71 mg, 0.57 mmol), the title compound was obtained after purification *via* flash column chromatography (25 → 50% ethyl acetate/hexanes) as a pale yellow solid (180 mg, 91%). **R**$_f$ = 0.36 (40% ethyl acetate/hexanes); **mp** = 272–274 C; **^{1}H NMR** (500 MHz, DMSO-d_6) δ 11.15 (s, 1H), 7.67 – 7.63 (m, 2H), 7.53 – 7.37 (m, 4H), 6.94 (d, J = 7.0 Hz, 1H), 5.16 (dd, J = 12.7, 5.4 Hz, 1H), 2.91 (ddd, J = 15.8, 12.4, 5.8 Hz, 1H), 2.67 – 2.53 (m, 2H), 2.37 (s, 3H), 2.14 – 2.04 (m, 1H); **^{13}C NMR** (126 MHz, DMSO) δ 172.8, 169.9, 166.7, 166.5, 140.1, 139.2, 135.9, 135.2, 132.6, 132.4, 131.0, 130.6, 130.3, 127.8, 124.8, 119.7, 79.2, 49.0, 31.0, 21.9, 20.8; **IR** (neat) 3179 (N-H), 2920, 1769 (C=O), 1731 (C=O), 1694 (C=O), 1390, 1207, 747 cm^{-1}; **HRMS** calculated for $C_{20}H_{17}N_2O_4S$: 381.0909, found: 381.0911 $[M+H]^+$.

2-(2,6-Dioxopiperidin-3-yl)-4-(*p*-tolylthio)isoindoline-1,3-dione (7e). Following the general procedure for the synthesis of thioether derivatives, using the coupling partner 4-methylbenzenethiol (71 mg, 0.57 mmol), the title compound was obtained after purification *via* flash column chromatography (35% ethyl acetate/hexanes) as a pale yellow solid (102 mg, 52%). **R**$_f$ = 0.40 (40% ethyl acetate/hexanes); **mp** = 256–258 °C; **^{1}H NMR** (500 MHz, DMSO) δ 11.11 (s, 1H), 7.68 – 7.58 (m, 3H), 7.52 (t, J = 6.0 Hz, 2H), 7.39 (dt, J = 8.4, 4.4 Hz, 1H), 6.73 (p, J = 3.7 Hz, 1H), 5.16 (dd, J = 12.8, 5.4 Hz, 1H), 2.91 (ddd, J = 16.8, 13.8, 5.4 Hz, 1H), 2.66 – 2.53 (m, 2H), 2.34 (s, 3H), 2.13 – 2.06 (m, 1H); **^{13}C NMR** (126 MHz, DMSO) δ 172.8, 169.9, 166.7, 166.6, 142.8, 138.4, 136.8, 135.3, 132.6, 131.5, 131.01, 129.8, 127.9, 127.1, 124.9, 119.6, 49.0, 31.0, 21.9, 20.2; **IR** (neat) 3199 (N-H), 3076, 2915, 1769 (C=O), 1730 (C=O), 1694 (C=O), 1458, 1389, 1257, 893, 745 cm^{-1}; **HRMS** calculated $C_{20}H_{17}N_2O_4S$: 381.0909, found: 381.0906 $[M+H]^+$.

4-((4-(*tert*-Butyl)phenyl)thio)-2-(2,6-dioxopiperidin-3-yl)isoindoline-1,3-dione (7f). Following the general procedure for the synthesis of thioether derivatives, using the coupling partner 4-(*tert*-butyl)-benzenethiol (118 µL), the title compound xx was obtained after purification *via* flash column chromatography (20 → 40% ethyl acetate/hexanes) as a pale yellow solid (212 mg, 97%). **R**$_f$ = 0.32 (40% ethyl acetate/hexanes); **mp** = 268–270 °C; **^{1}H NMR** (500 MHz, $CDCl_3$) δ 8.36 (s, 1H), 7.61 – 7.46 (m, 5H), 7.42 (t, J = 7.7 Hz, 1H), 6.95 (d, J = 8.1 Hz, 1H), 5.02 (dd, J = 12.1, 5.1 Hz, 1H), 2.95 – 2.73 (m, 3H), 2.16 (dd, J = 7.4, 5.2 Hz, 1H), 1.36 (s, 9H); **^{13}C NMR** (126 MHz, $CDCl_3$) δ 171.2, 168.2, 167.1, 167.0, 153.7, 141.8, 135.8, 134.4, 132.7, 131.1, 127.4, 125.2, 125.1, 119.7, 49.4, 35.0, 31.5, 31.3, 22.8; **IR** (neat, cm^{-1}) 3234 (N-H), 3096, 2959, 1769 (C=O), 1701 (C=O), 1489, 1388, 1257, 1115, 891, 738; **HRMS** calculated $C_{23}H_{23}N_2O_4S$: 423.1379, found: 423.1370 $[M+H]^+$.

2-(2,6-Dioxopiperidin-3-yl)-4-((4-(trifluoromethyl)phenyl)thio)isoindoline-1,3-dione (7g). Following the general procedure for the synthesis of thioether derivatives, using 4-trifluoromethylbenzenethiol (93 mg), the title compound was obtained after purification *via* flash column chromatography (40% ethyl acetate/hexanes) as a yellow solid (157 mg, 70%). $\mathbf{R_f}$ = 0.33 (40% ethyl acetate/hexanes); **mp** = 223–226 °C; **^{1}H NMR** (500 MHz, $CDCl_3$) δ 8.01 (s, 1H), 7.75 – 7.69 (m, 4H), 7.65 (d, J = 7.3 Hz, 1H), 7.51 (dd, J = 8.1, 7.3 Hz, 1H), 7.05 (d, J = 8.2 Hz, 1H), 5.01 (dd, J = 12.4, 5.3 Hz, 1H), 3.02 – 2.67 (m, 3H), 2.22 – 2.13 (m, 1H); **^{13}C NMR** (126 MHz, $CDCl_3$) δ 170.8, 167.9, 166.8, 166.7, 135.4, 134.8, 132.1, 127.0 (q, J = 3.8 Hz), 120.9, 55.9, 30.5, 21.9; **^{19}F NMR** ($CDCl_3$, MHz): δ -59.36; **IR** (neat): 3196 (N-H), 3103, 2900, 1707 (C=O), 1598, 1397, 1318, 1138, 842, 736 cm^{-1}; **HRMS** calculated: 435.0626, found: 435.0619 $[M+H]^+$.

2-(2,6-Dioxopiperidin-3-yl)-4-((5-(trifluoromethyl)pyridin-2-yl)thio)isoindoline-1,3-dione (7h). Following the general procedure for the synthesis of thioether derivatives, using the coupling partner 5-(trifluoromethyl)pyridine-2-thiol (102 mg), the title compound xx was obtained after purification *via* flash column chromatography (20 → 40 % ethyl acetate/hexanes) as a yellow solid (70 mg, 31%). $\mathbf{R_f}$ = 0.43 (40% ethyl acetate/hexanes); **mp** = 262–265 °C; **^{1}H NMR** (500 MHz, $CDCl_3$) δ 8.63 (d, J = 1.2 Hz, 1H), 8.00 (s, 1H), 7.92 – 7.85 (m, 2H), 7.82 (dd, J = 8.4, 2.3 Hz, 1H), 7.74 (t, J = 7.7 Hz, 1H), 7.45 (d, J = 8.4 Hz, 1H), 4.95 (dd, J = 12.5, 5.4 Hz, 1H), 2.93 – 2.85 (m, 1H), 2.84 – 2.66 (m, 2H), 2.15 – 2.10 (m, 1H); **^{13}C NMR** (126 MHz, $CDCl_3$) δ 170.6, 167.6, 166.3, 165.7, 161.3, 146.8 (q, J = 4.0 Hz), 139.3, 134.6, 134.5, 133.9 (q, J = 3.4 Hz), 133.3, 130.9, 130.6, 123.7, 123.1, 49.4, 31.3, 22.5.; **IR** (neat): 3196 (N-H), 2901, 1707 (C=O), 1598, 1454, 1318, 1138, 842, 736 cm^{-1}; **HRMS** calculated for $C_{19}H_{13}N_3O_4F_3S$: 436.0579, found: 436.0576 $[M+H]^+$.

2-(2,6-Dioxopiperidin-3-yl)-4-((4-methoxyphenyl)thio)isoindoline-1,3-dione (7i). Following the general procedure for the synthesis of thioether derivatives, using the coupling partner 4-mercaptoanisole (56 µL), the title compound was obtained after purification *via* flash column chromatography (30 → 50% ethyl acetate/hexanes) as a yellow solid (148 mg, 72%). $\mathbf{R_f}$ = 0.40 (40% ethyl acetate/hexanes); **mp** = 196–198 °C; **^{1}H NMR** (500 MHz, DMSO-d_6) δ 11.15 (s, 1H), 7.68 – 7.54 (m, 4H), 7.18 – 7.10 (m, 2H), 6.88 (dd, J = 7.7, 1.2 Hz, 1H), 5.17 (dd, J = 12.8, 5.4 Hz, 1H), 3.85 (s, 3H), 2.91 (ddd, J = 16.7, 13.7, 5.4 Hz, 1H), 2.65 – 2.52 (m, 2H), 2.09 (ddd, J = 9.7, 5.7, 2.6 Hz, 1H); **^{13}C NMR** (126 MHz, DMSO-d_6) δ 172.8, 169.8, 166.7, 166.5, 161.0, 140.4, 137.6, 135.1, 132.3, 130.1, 124.5, 119.4, 117.9, 116.1, 55.5, 49.0, 31.0, 22.0; **IR** (neat) 3196 (N-H), 3095, 2942, 2688 (OCH_3 C-H), 1766 (C=O), 1732 (C=O), 1695 (C=O), 1593, 1392, 1252, 1198, 741 cm^{-1}; **HRMS** calculated for $C_{20}H_{17}N_2O_4S$: 397.0858, found 397.0862 $[M+H]^+$.

2-(2,6-Dioxopiperidin-3-yl)-4-((4-(methylsulfanyl)phenyl)thio)isoindoline-1,3-dione (7j). Following the general procedure for the synthesis of thioether derivatives, using the coupling partner 4-(methylsulfanyl)thiophenol (45 mg), the title compound was obtained after purification *via* flash column chromatography (30 → 50% ethyl acetate/hexanes) as a yellow solid (42 mg, 38%). $\mathbf{R_f}$ = 0.44 (40% ethyl acetate/hexanes); **mp** = 242-244 °C; **^{1}H NMR** (400 MHz, $CDCl_3$) δ 8.20 = (s, 1H, COCN-H), 7.59 – 7.40 (m, 4H, Ar-H), 7.36 – 7.29 (m, 2H, Ar-H), 6.98 – 6.92 (m, 1H, Ar-H), 5.01 (dd, J = 12.1, 5.4 Hz, 1H), 2.99 – 2.68 (m, 3H), 2.53 (s,

3H), 2.22 – 2.10 (m, 1H); **^{13}C NMR** (75 MHz, $CDCl_3$) δ 171.1, 168.1, 167.0, 142.3, 141.6, 136.4, 134.5, 132.7, 131.0, 127.20, 124.1, 119.9, 49.4, 31.5, 22.8, 15.2; **IR** (neat) 3213 (N-H), 3091, 1768 (C=O), 1699 (C=O), 1385, 1256 1128 749 cm^{-1}; **HRMS** calculated for $C_{20}H_{17}N_2O_4S$: 413.0630, found: 413.0627 $[M+H]^+$.

4-(Benzylthio)-2-(2,6-dioxopiperidin-3-yl)isoindoline-1,3-dione (7k) Following the general procedure for the synthesis of thioether derivatives, using the coupling partner benzyl thiol (67 µL), the title compound was obtained after purification *via* flash column chromatography (20 → 60% ethyl acetate/hexanes) as a yellow solid (127 mg, 64%). **R**$_f$ = 0.35 (40% ethyl acetate/hexanes); **mp** = 223–225 °C; **^{1}H NMR** (500 MHz, DMSO-d_6) δ 11.12 (s, 1H), 7.82 (d, J = 8.1 Hz, 1H), 7.76 (t, J = 7.7 Hz, 1H), 7.63 (d, J = 7.1 Hz, 1H), 7.48 (d, J = 7.2 Hz, 2H), 7.35 (t, J = 7.5 Hz, 2H), 7.28 (t, J = 7.3 Hz, 1H), 5.11 (dd, J = 12.9, 5.4 Hz, 1H), 4.45 (s, 2H), 2.88 (ddd, J = 17.1, 14.0, 5.4 Hz, 1H), 2.67 – 2.52 (m, 2H), 2.10 – 2.00 (m, 1H); **^{13}C NMR** (126 MHz, DMSO-d_6) δ 172.8, 169.9, 166.7, 166.6, 138.4, 136.1, 134.9, 132.5, 130.7, 129.0, 128.6, 127.4, 125.3, 119.1, 79.2, 48.90, 34.0, 30.9, 21.9; **IR** (neat) 3196 (N-H), 3101, 3021, 1761, 1702 (C=O), 1598, 1458, 1395, 1326, 1259, 1197, 1019, 736 cm^{-1}; **HRMS** calculated for $C_{20}H_{17}N_2O_4S$: 418.0862, found: 418.0865 $[M+H]^+$.

4-(Butylthio)-2-(2,6-dioxopiperidin-3-yl)isoindoline-1,3-dione (7l). Following the general procedure for the synthesis of thioether derivatives, using the coupling partner 1-buntanethiol (61 µL), the title compound was obtained after purification *via* flash column chromatography (ethyl acetate/hexanes 20:80 → 50:50) as a yellow solid (146 mg, 81%). **R**$_f$ = 0.57 (50% ethyl acetate/hexanes); **mp** = 192–194 °C; **^{1}H NMR** (500 MHz, $CDCl_3$) δ 8.29 (s, 1H), 7.59 (dd, J = 18.7, 7.2 Hz, 2H), 7.50 (d, J = 7.6 Hz, 1H), 4.97 (dd, J = 11.4, 4.7 Hz, 1H), 3.04 (t, J = 7.0 Hz, 2H), 2.91 – 2.71 (m, 3H), 2.12 (d, J = 5.5 Hz, 1H), 1.74 (quint, 2H), 1.52 (app. dd, J = 14.2, 7.0 Hz, 2H), 0.96 (t, J = 7.1 Hz, 3H); **^{13}C NMR** (126 MHz, $CDCl_3$) δ 171.2, 168.2, 167.0, 166.9, 140.5, 134.4, 133.1, 130.0, 126.2, 119.2, 49.3, 31.5, 30.6, 30.4, 22.8, 22.2, 13.7; **IR** (neat) 3198 (N-H), 3095, 2905, 1769 (C=O), 1697 (C=O), 1459, 1389, 1322, 1260, 1199, 1183, 1116, 1014, 893, 742 cm^{-1}; **HRMS** calculated for $C_{17}H_{19}N_2O_4S$: 347.1066, found: 347.1068 $[M+H]^+$.

4-(*Tert*-butylthio)-2-(2,6-dioxopiperidin-3-yl)isoindoline-1,3-dione (7m). Following the general procedure for the synthesis of thioether derivatives, using the coupling partner 2-methyl-2-propanethiol (65 µL), the title compound was obtained after purification *via* flash column chromatography (20:80 → 50:50 ethyl acetate/hexanes) as a yellow solid (178 mg, 99%). **R**$_f$ = 0.43 (40% ethyl acetate/hexanes); **mp** = 189–191 °C; **^{1}H NMR** (500 MHz, $CDCl_3$) δ 8.01 (s, 1H), 7.85 (dd, J = 7.9, 0.9 Hz, 1H), 7.82 (dd, J = 7.4, 0.9 Hz, 1H), 7.67 (t, J = 7.6 Hz, 1H), 4.98 (dd, J = 12.4, 5.4 Hz, 1H), 2.94 – 2.87 (m, 2H), 2.83 (td, J = 12.7, 12.2, 3.9 Hz, 1H), 2.79 – 2.70 (m, 1H), 2.18 – 2.11 (m, 2H), 1.43 (s, 8H); **^{13}C NMR** (126 MHz, $CDCl_3$) δ 170.9, 167.9, 166.6, 166.4, 142.1, 135.2, 133.7, 133.4, 132.4, 122.9, 49.5, 48.6, 31.5, 31.3, 22.7; **IR** (neat): 3185 (N-H), 1770 (C=O), 1697 (C=O), 1602, 1460, 1391, 1200, 1118, 743 cm^{-1}; **HRMS** calculated for $C_{17}H_{19}N_2O_4S$: 347.1066, found: 347.1068 $[M+H]^+$.

4-(Cyclohexylthio)-2-(2,6-dioxopiperidin-3-yl)isoindoline-1,3-dione (7n). Following the general procedure for the synthesis of thioether derivatives, using the coupling partner cyclohexanethiol (90 µL), the title compound was obtained after purification *via* flash column

chromatography (30% → 50% ethyl acetate/hexanes) as a pale yellow solid (170 mg, 88%). **R_f** = 0.27 (30% ethyl acetate/hexanes); **mp** = 205–207 °C. **^{1}H NMR** (600 MHz, $CDCl_3$) δ 7.95 (s, 1H), 7.65 – 7.58 (m, 2H), 7.55 (dd, J = 7.9, 0.9 Hz, 1H), 4.96 (dd, J = 12.5, 5.4 Hz, 1H), 3.45 (dd, J = 6.9, 3.7 Hz, 1H), 2.93 – 2.88 (m, 1H), 2.83 (dd, J = 11.1, 2.4 Hz, 1H), 2.77 – 2.70 (m, 1H), 2.18 – 2.07 (m, 3H), 1.89 – 1.81 (m, 2H), 1.72 – 1.66 (m, 1H), 1.58 – 1.50 (m, 2H), 1.48 – 1.39 (m, 2H), 1.38 – 1.29 (m, 1H). **^{13}C NMR** (126 MHz, $CDCl_3$) δ 170.8, 167.93, 167.0, 166.9, 139.8, 134.3, 133.3, 131.2, 126.6, 119.5, 49.3, 43.3, 32.96, 32.93, 31.5, 26.1, 25.8, 22.8; **IR** (neat) 3190 (N-H), 3077, 2922, 1769 (C=O), 1697 (C=O), 1389, 1257 893, 741 cm^{-1}; **HRMS** (ESI) calculated for $C_{19}H_{21}N_2O_4S$: 373.1222, found: 373.1225 $[M+H]^+$.

4-(Adamantylthio)-2-(2,6-dioxopiperidin-3-yl)isoindoline-1,3-dione (7o). Following the general procedure for the synthesis of thioether derivatives, using the coupling partner 1-adamantanethiol (98 mg), the title compound was obtained after purification *via* flash column chromatography (ethyl acetate/hexanes 20:80 → 50:50) as a pale yellow solid (204 mg, 92%). **R_f** = 0.41 (40% ethyl acetate/hexanes); **mp** could not be determined (turned black at *ca.* 140 °C, presumably decomposed); **^{1}H NMR** (600 MHz, $CDCl_3$) δ 8.26 (s, 1H), 7.82 (t, J = 8.5 Hz, 2H), 7.64 (t, J = 7.6 Hz, 1H), 4.98 (dd, J = 12.3, 5.3 Hz, 1H), 2.94 – 2.69 (m, 3H), 2.14 (dd, J = 8.8, 3.9 Hz, 1H), 2.04 (s, 3H), 1.93 (s, 6H), 1.64 (q, J = 12.7 Hz, 6H).^{13}C NMR (151 MHz, $CDCl_3$) δ 171.1, 168.1, 166.6, 166.4, 143.9, 133.4, 133.4, 133.3, 132.6, 123.4, 51.4, 49.4, 43.8, 36.1, 31.5, 30.2, 22.7; **IR** (neat) 3256 (N-H), 3103, 2903, 2849, 1770, 1703 (C=O), 1457, 1382, 1256, 1192, 1117, 1035, 891, 740 cm^{-1}; **HRMS** calculated for $C_{23}H_{25}N_2O_4S$: 425.1535, found: 425.1525 $[M+H]^+$.

4-((4-(Tert-butyl)phenyl)thio)-2-(1-methyl-2,6-dioxopiperidin-3-yl)isoindoline-1,3-dione 7p). To a flame-dried Schlenk flask, thiothalidomide **8e** (100 mg, mmol, 1.0 equiv) and K_2CO_3 (66 mg, 0.47 mmol, 2.0 equiv) were suspended in DMF (1 mL) and cooled to 0 °C with continuous stirring. Methyl iodide (40 mg, 0.28 mmol, 1.2 equiv) was added slowly dropwise, the mixture was allowed to warm to room temperature and then stirred for a further 16 h. The reaction mixture was diluted with ethyl acetate (15 mL), washed with LiCl (1M, 15 mL) three times, and these aqueous fractions were extracted with additional ethyl acetate (15 mL). The combined organic layers were washed with brine (30 mL), dried over $MgSO_4$, filtered and concentrated under reduced pressure. The crude residue was subjected to purification by flash column chromatography (40% ethyl acetate/hexanes) to give the title compound as a pale yellow solid. **R_f** = 0.34 (40% ethyl acetate/hexanes). **mp** = 184-185 °C; **^{1}H NMR** (500 MHz, $CDCl_3$) δ 7.55 – 7.48 (m, 1H), 7.42 (dd, J = 8.1, 7.3 Hz, 1H), 6.97 – 6.93 (m, 1H), 5.03 – 4.96 (m, 1H), 3.22 (s, 1H), 3.03 – 2.96 (m, 1H), 2.87 – 2.74 (m, 1H), 2.17 – 2.09 (m, 1H), 1.36 (s, 2H); **^{13}C NMR** (126 MHz, $CDCl_3$) δ 171.3, 168.8, 167.3, 167.1, 153.7, 141.8, 135.8, 134.3, 132.7, 131.0, 127.4, 125.3, 125.1, 119.6, 50.1, 35.0, 32.0, 31.3, 27.4, 22.1; **IR** (neat) 2961, 1768 (C=O), 1709 (C=O), 1679 (C=O), 1602, 1456, 1389, 1115, 891, 739 cm^{-1}; **HRMS** (ESI) calculated for $C_{24}H_{25}N_2O_4S$: 437.1535, found: 437.1530 $[M+H]^+$.

Acknowledgements

The authors acknowledge the CMCA Research Facility at UWA. The ARC is gratefully acknowledged for support through DP200100860. The authors would like to thank xx and xx

for helpful discussion. Further NMR assistance from Dr. Gareth Nealon is gratefully acknowledged. Michael J. Nutt is a grateful recipient of financial support from an Australian RTP scholarship and the Ernest and Evelyn Havill-Shacklock scholarship.

(1) Vergara, T. R. C.; Samer, S.; Santos-Oliveira, J. R.; Giron, L. B.; Arif, M. S.; Silva-Freitas, M. L.; Cherman, L. A.; Treitsman, M. S.; Chebabo, A.; Sucupira, M. C. A.; Da-Cruz, A. M.; Diaz, R. S. Thalidomide Is Associated With Increased T Cell Activation and Inflammation in Antiretroviral-Naive HIV-Infected Individuals in a Randomised Clinical Trial of Efficacy and Safety. *EBioMedicine* **2017**, *23*, 59–67.

(2) Kumar, S.; Witzig, T. E.; Rajkumar, S. V. Thalidomide: Current Role in the Treatment of Non-Plasma Cell Malignancies. *Journal of Clinical Oncology*. J Clin Oncol 2004, pp 2477–2488.

(3) D'Amato, R. J.; Loughnan, M. S.; Flynn, E.; Folkman, J. Thalidomide Is an Inhibitor of Angiogenesis. *Proc. Natl. Acad. Sci. U. S. A.* **1994**, *91* (9), 4082–4085.

(4) Zhu, Y. X.; Kortuem, K. M.; Stewart, A. K. Molecular Mechanism of Action of Immune-Modulatory Drugs Thalidomide, Lenalidomide and Pomalidomide in Multiple Myeloma. *Leukemia and Lymphoma*. Taylor & Francis April 28, 2013, pp 683–687.

(5) Gribben, J. G.; Fowler, N.; Morschhauser, F. Mechanisms of Action of Lenalidomide in B-Cell Non-Hodgkin Lymphoma. *J. Clin. Oncol.* **2015**, *33* (25), 2803–2811.

(6) Mitsiades, N.; Mitsiades, C. S.; Poulaki, V.; Chauhan, D.; Richardson, P. G.; Hideshima, T.; Munshi, N. C.; Treon, S. P.; Anderson, K. C. Apoptotic Signaling Induced by Immunomodulatory Thalidomide Analogs in Human Multiple Myeloma Cells: Therapeutic Implications. *Blood* **2002**, *99* (12), 4525–4530.

(7) Jackson, G. H.; Davies, F. E.; Pawlyn, C.; Cairns, D. A.; Striha, A.; Collett, C.; Hockaday, A.; Jones, J. R.; Kishore, B.; Garg, M.; Williams, C. D.; Karunanithi, K.; Lindsay, J.; Jenner, M. W.; Cook, G.; Russell, N. H.; Kaiser, M. F.; Drayson, M. T.; Owen, R. G.; Gregory, W. M.; Morgan, G. J. Lenalidomide Maintenance versus Observation for Patients with Newly Diagnosed Multiple Myeloma (Myeloma XI): A Multicentre, Open-Label, Randomised, Phase 3 Trial. *Lancet Oncol.* **2019**, *20* (1), 57–73.

(8) Talati, C.; Sallman, D.; List, A. Lenalidomide: Myelodysplastic Syndromes with Del(5q) and Beyond. *Seminars in Hematology*. W.B. Saunders July 1, 2017, pp 159–166.

(9) Okafor, M. C. Thalidomide for Erythema Nodosum Leprosum and Other Applications. *Pharmacotherapy* **2003**, *23* (4), 481–493.

(10) Vargesson, N. Thalidomide-Induced Limb Defects: Resolving a 50-Year-Old Puzzle. *BioEssays* **2009**, *31* (12), 1327–1336.

(11) Angers, S.; Li, T.; Yi, X.; MacCoss, M. J.; Moon, R. T.; Zheng, N. Molecular Architecture and Assembly of the DDB1-CUL4A Ubiquitin Ligase Machinery. *Nature* **2006**, *443* (7111), 590–593.

(12) Ito, T.; Ando, H.; Imamura, Y.; Yamaguchi, Y.; Handa, H.; Ito, T.; Ando, H.; Suzuki, T.; Ogura, T.; Hotta, K. Identification of a Primary Target of Thalidomide

Teratogenicity. *Science (80).* **2010**, *327* (5971), 1345–1350.

(13) Akuffo, A. A.; Alontaga, A. Y.; Metcalf, R.; Beatty, M. S.; Becker, A.; McDaniel, J. M.; Hesterberg, R. S.; Goodheart, W. E.; Gunawan, S.; Ayaz, M.; Yang, Y.; Rezaul Karim, M.; Orobello, M. E.; Daniel, K.; Guida, W.; Yoder, J. A.; Rajadhyaksha, A. M.; Schönbrunn, E.; Lawrence, H. R.; Lawrence, N. J.; Epling-Burnette, P. K. Ligand-Mediated Protein Degradation Reveals Functional Conservation among Sequence Variants of the CUL4-Type E3 Ligase Substrate Receptor Cereblon. *J. Biol. Chem.* **2018**, *293* (16), 6187–6200.

(14) Lupas, A. N.; Zhu, H.; Korycinski, M. The Thalidomide-Binding Domain of Cereblon Defines the CULT Domain Family and Is a New Member of the β-Tent Fold. *PLoS Comput. Biol.* **2015**, *11* (1).

(15) Chamberlain, P. P.; Lopez-Girona, A.; Miller, K.; Carmel, G.; Pagarigan, B.; Chie-Leon, B.; Rychak, E.; Corral, L. G.; Ren, Y. J.; Wang, M.; Riley, M.; Delker, S. L.; Ito, T.; Ando, H.; Mori, T.; Hirano, Y.; Handa, H.; Hakoshima, T.; Daniel, T. O.; Cathers, B. E. Structure of the Human Cereblon–DDB1–Lenalidomide Complex Reveals Basis for Responsiveness to Thalidomide Analogs. *Nat. Struct. Mol. Biol.* **2014**, *21* (9), 803–809.

(16) Petzold, G.; Fischer, E. S.; Thomä, N. H. Structural Basis of Lenalidomide-Induced CK1α Degradation by the CRL4 CRBN Ubiquitin Ligase. *Nature* **2016**, *532* (7597), 127–130.

(17) Sievers, Q. L.; Petzold, G.; Bunker, R. D.; Renneville, A.; Słabicki, M.; Liddicoat, B. J.; Abdulrahman, W.; Mikkelsen, T.; Ebert, B. L.; Thomä, N. H. Defining the Human C2H2 Zinc Finger Degrome Targeted by Thalidomide Analogs through CRBN. *Science (80-.).* **2018**, *362* (6414), eaat0572. https://doi.org/10.1126/science.aat0572.

(18) Matyskiela, M. E.; Couto, S.; Zheng, X.; Lu, G.; Hui, J.; Stamp, K.; Drew, C.; Ren, Y.; Wang, M.; Carpenter, A.; Lee, C. W.; Clayton, T.; Fang, W.; Lu, C. C.; Riley, M.; Abdubek, P.; Blease, K.; Hartke, J.; Kumar, G.; Vessey, R.; Rolfe, M.; Hamann, L. G.; Chamberlain, P. P. SALL4 Mediates Teratogenicity as a Thalidomide-Dependent Cereblon Substrate. *Nat. Chem. Biol.* **2018**, *14* (10), 981–987. https://doi.org/10.1038/s41589-018-0129-x.

(19) Sperling, A. S.; Burgess, M.; Keshishian, H.; Gasser, J. A.; Bhatt, S.; Jan, M.; Słabicki, M.; Sellar, R. S.; Fink, E. C.; Miller, P. G.; Liddicoat, B. J.; Sievers, Q. L.; Sharma, R.; Adams, D. N.; Olesinski, E. A.; Fulciniti, M.; Udeshi, N. D.; Kuhn, E.; Letai, A.; Munshi, N. C.; Carr, S. A.; Ebert, B. L. Patterns of Substrate Affinity, Competition, and Degradation Kinetics Underlie Biological Activity of Thalidomide Analogs. *Blood* **2019**, *134* (2), 160–170. https://doi.org/10.1182/blood.2019000789.

(20) Qu, Z.; Jiang, C.; Wu, J.; Ding, Y. Lenalidomide Induces Apoptosis and Inhibits Angiogenesis via Caspase-3 and VEGF in Hepatocellular Carcinoma Cells. *Mol. Med. Rep.* **2016**, *14* (5), 4781–4786. https://doi.org/10.3892/mmr.2016.5797.

(21) Chen, Y.-Y. Thalidomide-Based Multidisciplinary Treatment for Patients with Advanced Hepatocellular Carcinoma: A Retrospective Analysis. *World J. Gastroenterol.* **2012**, *18* (5), 466. https://doi.org/10.3748/wjg.v18.i5.466.

(22) Woo, K.; Stewart, S. G.; Kong, G. S.; Finch-Edmondson, M. L.; Dwyer, B. J.; Yeung, S. Y.; Abraham, L. J.; Kampmann, S. S.; Diepeveen, L. A.; Passman, A. M. M.;

Elsegood, C. L.; Tirnitz-Parker, J. E. E.; Callus, B. A.; Olynyk, J. K.; Yeoh, G. C. T. Identification of a Thalidomide Derivative That Selectively Targets Tumorigenic Liver Progenitor Cells and Comparing Its Effects with Lenalidomide and Sorafenib. *Eur. J. Med. Chem.* **2016**, *120*, 275–283. https://doi.org/10.1016/j.ejmech.2016.03.015.

(23) El-Zahabi, M. A.; Sakr, H.; El-Adl, K.; Zayed, M.; Abdelraheem, A. S.; Eissa, S. I.; Elkady, H.; Eissa, I. H. Design, Synthesis, and Biological Evaluation of New Challenging Thalidomide Analogs as Potential Anticancer Immunomodulatory Agents. *Bioorg. Chem.* **2020**, *104*, 104218. https://doi.org/10.1016/j.bioorg.2020.104218.

(24) Fitzmaurice, C.; Allen, C.; Barber, R. M.; Barregard, L.; Bhutta, Z. A.; Brenner, H.; Dicker, D. J.; Chimed-Orchir, O.; Dandona, R.; Dandona, L.; Fleming, T.; Forouzanfar, M. H.; Hancock, J.; Hay, R. J.; Hunter-Merrill, R.; Huynh, C.; Hosgood, H. D.; Johnson, C. O.; Jonas, J. B.; Khubchandani, J.; Kumar, G. A.; Kutz, M.; Lan, Q.; Larson, H. J.; Liang, X.; Lim, S. S.; Lopez, A. D.; MacIntyre, M. F.; Marczak, L.; Marquez, N.; Mokdad, A. H.; Pinho, C.; Pourmalek, F.; Salomon, J. A.; Sanabria, J. R.; Sandar, L.; Sartorius, B.; Schwartz, S. M.; Shackelford, K. A.; Shibuya, K.; Stanaway, J.; Steiner, C.; Sun, J.; Takahashi, K.; Vollset, S. E.; Vos, T.; Wagner, J. A.; Wang, H.; Westerman, R.; Zeeb, H.; Zoeckler, L.; Abd-Allah, F.; Ahmed, M. B.; Alabed, S.; Alam, N. K.; Aldhahri, S. F.; Alem, G.; Alemayohu, M. A.; Ali, R.; Al-Raddadi, R.; Amare, A.; Amoako, Y.; Artaman, A.; Asayesh, H.; Atnafu, N.; Awasthi, A.; Saleem, H. B.; Barac, A.; Bedi, N.; Bensenor, I.; Berhane, A.; Bernabé, E.; Betsu, B.; Binagwaho, A.; Boneya, D.; Campos-Nonato, I.; Castañeda-Orjuela, C.; Catalá-López, F.; Chiang, P.; Chibueze, C.; Chitheer, A.; Choi, J. Y.; Cowie, B.; Damtew, S.; Das Neves, J.; Dey, S.; Dharmaratne, S.; Dhillon, P.; Ding, E.; Driscoll, T.; Ekwueme, D.; Endries, A. Y.; Farvid, M.; Farzadfar, F.; Fernandes, J.; Fischer, F.; Ghiwot, T. T.; Gebru, A.; Gopalani, S.; Hailu, A.; Horino, M.; Horita, N.; Husseini, A.; Huybrechts, I.; Inoue, M.; Islami, F.; Jakovljevic, M.; James, S.; Javanbakht, M.; Jee, S. H.; Kasaeian, A.; Kedir, M. S.; Khader, Y. S.; Khang, Y. H.; Kim, D.; Leigh, J.; Linn, S.; Lunevicius, R.; El Razek, H. M. A.; Malekzadeh, R.; Malta, D. C.; Marcenes, W.; Markos, D.; Melaku, Y. A.; Meles, K. G.; Mendoza, W.; Mengiste, D. T.; Meretoja, T. J.; Miller, T. R.; Mohammad, K. A.; Mohammadi, A.; Mohammed, S.; Moradi-Lakeh, M.; Nagel, G.; Nand, D.; Le Nguyen, Q.; Nolte, S.; Ogbo, F. A.; Oladimeji, K. E.; Oren, E.; Pa, M.; Park, E. K.; Pereira, D. M.; Plass, D.; Qorbani, M.; Radfar, A.; Rafay, A.; Rahman, M.; Rana, S. M.; Søreide, K.; Satpathy, M.; Sawhney, M.; Sepanlou, S. G.; Shaikh, M. A.; She, J.; Shiue, I.; Shore, H. R.; Shrime, M. G.; So, S.; Soneji, S.; Stathopoulou, V.; Stroumpoulis, K.; Sufiyan, M. B.; Sykes, B. L.; Tabarés-Seisdedos, R.; Tadese, F.; Tedla, B. A.; Tessema, G. A.; Thakur, J. S.; Tran, B. X.; Ukwaja, K. N.; Chudi Uzochukwu, B. S.; Vlassov, V. V.; Weiderpass, E.; Wubshet Terefe, M.; Yebyo, H. G.; Yimam, H. H.; Yonemoto, N.; Younis, M. Z.; Yu, C.; Zaidi, Z.; Zaki, M. E. S.; Zenebe, Z. M.; Murray, C. J. L.; Naghavi, M. Global, Regional, and National Cancer Incidence, Mortality, Years of Life Lost, Years Lived with Disability, and Disability-Adjusted Life-Years for 32 Cancer Groups, 1990 to 2015: A Systematic Analysis for the Global Burden of Disease Study Global Burden of Disease Cancer Collaboration. *JAMA Oncology*. American Medical Association April 1, 2017, pp 524–548. https://doi.org/10.1001/jamaoncol.2016.5688.

(25) World Health Organization (WHO). Newsroom, Fact Sheets, Cancer https://www.who.int/news-room/fact-sheets/detail/cancer (accessed Apr 21, 2020).

(26) Dai, Q.; Zhang, C.; Yuan, Z.; Sun, Q.; Jiang, Y. Current Discovery Strategies for Hepatocellular Carcinoma Therapeutics. *Expert Opin. Drug Discov.* **2020**, *15* (2), 243–

258. https://doi.org/10.1080/17460441.2020.1696769.

(27) Llovet, J. M.; Ricci, S.; Mazzaferro, V.; Hilgard, P.; Gane, E.; Blanc, J.-F.; de Oliveira, A. C.; Santoro, A.; Raoul, J.-L.; Forner, A.; Schwartz, M.; Porta, C.; Zeuzem, S.; Bolondi, L.; Greten, T. F.; Galle, P. R.; Seitz, J.-F.; Borbath, I.; Häussinger, D.; Giannaris, T.; Shan, M.; Moscovici, M.; Voliotis, D.; Bruix, J. Sorafenib in Advanced Hepatocellular Carcinoma. *N. Engl. J. Med.* **2008**, *359* (4), 378–390. https://doi.org/10.1056/NEJMoa0708857.

(28) Stewart, S. G.; Ho, L. A.; Polomska, M. E.; Percival, A. T.; Yeoh, G. C. T. Rapid Evaluation of Antrodia Camphorata Natural Products and Derivatives in Tumourigenic Liver Progenitor Cells with a Novel Cell Proliferation Assay. *ChemMedChem* **2009**, *4* (10), 1657–1667. https://doi.org/10.1002/cmdc.200900238.

(29) Lowes, K. N.; Brennan, B. A.; Yeoh, G. C.; Olynyk, J. K. Oval Cell Numbers in Human Chronic Liver Diseases Are Directly Related to Disease Severity. *Am. J. Pathol.* **1999**, *154* (2), 537–541. https://doi.org/10.1016/S0002-9440(10)65299-6.

(30) Sun, B.; Karin, M. Inflammation and Liver Tumorigenesis. *Front. Med.* **2013**, *7*, 242–254. https://doi.org/10.1007/s11684-013-0256-4.

(31) Knight George Yeoh, B. C. TNF/LTα Double Knockout Mice Display Abnormal Inflammatory and Regenerative Responses to Acute and Chronic Liver Injury. *Cell Tissue Res* **2005**, *319*, 61–70. https://doi.org/10.1007/s00441-004-1003-6.

(32) Knight, B. B.; Yeoh, G. C. T.; Husk, K. L.; Ly, T.; Abraham, L. J.; Yu, C.; Rhim, J. A.; Fausto, N. Impaired Preneoplastic Changes and Liver Tumor Formation in Tumor Necrosis Factor Receptor Type 1 Knockout Mice. *J. Exp. Med.* **2000**, *192* (12), 1809–1818.

(33) He, G.; Dhar, D.; Nakagawa, H.; Font-Burgada, J.; Ogata, H.; Jiang, Y.; Shalapour, S.; Seki, E.; Yost, S. E.; Jepsen, K.; Frazer, K. A.; Harismendy, O.; Hatziapostolou, M.; Iliopoulos, D.; Suetsugu, A.; Hoffman, R. M.; Tateishi, R.; Koike, K.; Karin, M. Identification of Liver Cancer Progenitors Whose Malignant Progression Depends on Autocrine IL-6 Signaling. *Cell* **2013**, *155* (2), 384. https://doi.org/10.1016/j.cell.2013.09.031.

(34) Stewart, S. G.; Spagnolo, D.; Polomska, M. E.; Sin, M.; Karimi, M.; Abraham, L. J. Synthesis and TNF Expression Inhibitory Properties of New Thalidomide Analogues Derived via Heck Cross Coupling. *Bioorganic Med. Chem. Lett.* **2007**, *17* (21), 5819–5824. https://doi.org/10.1016/j.bmcl.2007.08.042.

(35) Stewart, S. G.; Braun, C. J.; Ng, S.-L.; Polomska, M. E.; Karimi, M.; Abraham, L. J. New Thalidomide Analogues Derived through Sonogashira or Suzuki Reactions and Their TNF Expression Inhibition Profiles. *Bioorg. Med. Chem.* **2010**, *18* (2), 650–662. https://doi.org/10.1016/j.bmc.2009.12.001.

(36) Yeung, S. Y.; Kampmann, S.; Stubbs, K. A.; Skelton, B. W.; Kaskow, B. J.; Abraham, L. J.; Stewart, S. G.; Viaud-Massuard, M.-C.; Hashimoto, Y. Novel Thalidomide Analogues with Potent NF$κ$B and TNF Expression Inhibition. *Med. Chem. Commun.* **2011**, *2*, 1073–1078. https://doi.org/10.1039/c1md00184a.

(37) Keifer, J. A.; Guttridge, D. C.; Ashburner, B. P.; Baldwin, A. S. Inhibition of NF-KB Activity by Thalidomide through Suppression of IκB Kinase Activity. *J. Biol. Chem.* **2001**, *276* (25), 22382–22387. https://doi.org/10.1074/jbc.M100938200.

(38) Tan, W.; Luo, X.; Li, W.; Zhong, J.; Cao, J.; Zhu, S.; Chen, X.; Zhou, R.; Shang, C.; Chen, Y. TNF-α Is a Potential Therapeutic Target to Overcome Sorafenib Resistance in Hepatocellular Carcinoma. *EBioMedicine* **2019**, *40*, 446–456. https://doi.org/10.1016/j.ebiom.2018.12.047.

(39) Knight, B.; Yeoh, G. C. TNF/LTα Double Knockout Mice Display Abnormal Inflammatory and Regenerative Responses to Acute and Chronic Liver Injury. *Cell Tissue Res.* **2005**, *319* (1), 61–70. https://doi.org/10.1007/s00441-004-1003-6.

(40) Capitosti, S. M.; Hansen, T. P.; Brown, M. L. Facile Synthesis of an Azido-Labeled Thalidomide Analogue. *Org. Lett.* **2003**, *5* (16), 2865–2867. https://doi.org/10.1021/ol034906w.

(41) Schwartz, W. T. Process for the Preparation of Phenoxy Phthalic Anhydrides. US4827000, 1987.

(42) Itoh, T.; Mase, T. A General Palladium-Catalyzed Coupling of Aryl Bromides/Triflates and Thiols. *Org. Lett.* **2004**, *6* (24), 4587–4590. https://doi.org/10.1021/ol047996t.

(43) Xiao, D.; Wang, Y. jie; Hu, X. bei; Kan, W. juan; Zhang, Q.; Jiang, X.; Zhou, Y. bo; Li, J.; Lu, W. Design, Synthesis and Biological Evaluation of the Thioether-Containing Lenalidomide Analogs with Anti-Proliferative Activities. *Eur. J. Med. Chem.* **2019**, *176*, 419–430. https://doi.org/10.1016/j.ejmech.2019.05.035.

(44) Wang, Y.; Mi, T.; Li, Y.; Kan, W.; Xu, G.; Li, J.; Zhou, Y.; Li, J.; Jiang, X. Design, Synthesis and Biological Evaluation of Thioether-Containing Lenalidomide and Pomalidomide Derivatives with Anti-Multiple Myeloma Activity. *Eur. J. Med. Chem.* **2020**, 112912. https://doi.org/10.1016/j.ejmech.2020.112912.

(45) Wang, L.; He, W.; Yu, Z. Transition-Metal Mediated Carbon–Sulfur Bond Activation and Transformations. *Chem. Soc. Rev.* **2013**, *42* (2), 599–621. https://doi.org/10.1039/C2CS35323G.

(46) Wang, Y.; Mi, T.; Li, Y.; Kan, W.; Xu, G.; Li, J.; Zhou, Y.; Li, J.; Jiang, X. Design, Synthesis and Biological Evaluation of Thioether-Containing Lenalidomide and Pomalidomide Derivatives with Anti-Multiple Myeloma Activity. *Eur. J. Med. Chem.* **2020**, 112912. https://doi.org/10.1016/j.ejmech.2020.112912.

(47) Hansen, J. D.; Correa, M.; Nagy, M. A.; Alexander, M.; Plantevin, V.; Grant, V.; Whitefield, B.; Huang, D.; Kercher, T.; Harris, R.; Narla, R. K.; Leisten, J.; Tang, Y.; Moghaddam, M.; Ebinger, K.; Piccotti, J.; Havens, C. G.; Cathers, B.; Carmichael, J.; Daniel, T.; Vessey, R.; Hamann, L. G.; Leftheris, K.; Mendy, D.; Baculi, F.; LeBrun, L. A.; Khambatta, G.; Lopez-Girona, A. Discovery of CRBN E3 Ligase Modulator CC-92480 for the Treatment of Relapsed and Refractory Multiple Myeloma. *J. Med. Chem.* **2020**. https://doi.org/10.1021/acs.jmedchem.9b01928.

(48) Pinter, M.; Wichlas, M.; Schmid, K.; Plank, C.; Müller, C.; Wrba, F.; Peck-Radosavljevic, M. Thalidomide in Advanced Hepatocellular Carcinoma as Antiangiogenic Treatment Approach: A Phase I/II Trial. *Eur. J. Gastroenterol. Hepatol.* **2008**, *20* (10), 1012–1019. https://doi.org/10.1097/MEG.0b013e3283036740.

(49) Muller, G. W.; Chen, R.; Huang, S. Y.; Corral, L. G.; Wong, L. M.; Patterson, R. T.; Chen, Y.; Kaplan, G.; Stirling, D. I. Amino-Substituted Thalidomide Analogs: Potent Inhibitors of TNF-?? Production. *Bioorganic Med. Chem. Lett.* **1999**, *9* (11), 1625–

1630. https://doi.org/10.1016/S0960-894X(99)00250-4.

(50) Zhou, B.; Hu, J.; Xu, F.; Chen, Z.; Bai, L.; Fernandez-Salas, E.; Lin, M.; Liu, L.; Yang, C.-Y.; Zhao, Y.; Mceachern, D.; Przybranowski, S.; Wen, B.; Sun, D.; Wang, S. Discovery of a Small-Molecule Degrader of Bromodomain and Extra-Terminal (BET) Proteins with Picomolar Cellular Potencies and Capable of Achieving Tumor Regression. **2017**. https://doi.org/10.1021/acs.jmedchem.6b01816.

(51) Steinebach, C.; Lindner, S.; Udeshi, N. D.; Mani, D. C.; Kehm, H.; Köpff, S.; Carr, S. A.; Gütschow, M.; Krönke, J. Homo-PROTACs for the Chemical Knockdown of Cereblon. *ACS Chem. Biol.* **2018**, *13* (9), 2771–2782. https://doi.org/10.1021/acschembio.8b00693.

(52) Chesi, M.; Matthews, G. M.; Garbitt, V. M.; Palmer, S. E.; Shortt, J.; Lefebure, M.; Stewart, A. K.; Johnstone, R. W.; Leif Bergsagel, P. Drug Response in a Genetically Engineered Mouse Model of Multiple Myeloma Is Predictive of Clinical Efficacy. *Blood* **2012**, *120* (2), 376–385. https://doi.org/10.1182/blood-2012-02-412783.

(53) Fink, E. C.; McConkey, M.; Adams, D. N.; Haldar, S. D.; Kennedy, J. A.; Guirguis, A. A.; Udeshi, N. D.; Mani, D. R.; Chen, M.; Liddicoat, B.; Svinkina, T.; Nguyen, A. T.; Carr, S. A.; Ebert, B. L. CrbnI391V Is Sufficient to Confer in Vivo Sensitivity to Thalidomide and Its Derivatives in Mice. *Blood* **2018**, *132* (14), 1535–1544. https://doi.org/10.1182/blood-2018-05-852798.

(54) Brodt, P. Role of the Microenvironment in Liver Metastasis: From Pre-to Prometastatic Niches. *Clin Cancer Res* **2016**, *22* (24). https://doi.org/10.1158/1078-0432.CCR-16-0460.

(55) Lee, J. W.; Stone, M. L.; Porrett, P. M.; Thomas, S. K.; Komar, C. A.; Li, J. H.; Delman, D.; Graham, K.; Gladney, W. L.; Hua, X.; Black, T. A.; Chien, A. L.; Majmundar, K. S.; Thompson, J. C.; Yee, S. S.; O'Hara, M. H.; Aggarwal, C.; Xin, D.; Shaked, A.; Gao, M.; Liu, D.; Borad, M. J.; Ramanathan, R. K.; Carpenter, E. L.; Ji, A.; de Beer, M. C.; de Beer, F. C.; Webb, N. R.; Beatty, G. L. Hepatocytes Direct the Formation of a Pro-Metastatic Niche in the Liver. *Nature*. Nature Publishing Group March 14, 2019, pp 249–252. https://doi.org/10.1038/s41586-019-1004-y.

(56) Yang, S.; Liu, G. Targeting the RAS/RAF/MEK/ERK Pathway in Hepatocellular Carcinoma. *Oncology Letters*. Spandidos Publications March 1, 2017, pp 1041–1047. https://doi.org/10.3892/ol.2017.5557.

(57) Luedde, T.; Schwabe, R. F. NF-KB in the Liver-Linking Injury, Fibrosis and Hepatocellular Carcinoma. *Nature Reviews Gastroenterology and Hepatology*. NIH Public Access February 2011, pp 108–118. https://doi.org/10.1038/nrgastro.2010.213.

(58) Li, J.; Lau, G. K. K.; Chen, L.; Dong, S. sui; Lan, H. Y.; Huang, X. R.; Li, Y.; Luk, J. M.; Yuan, Y. F.; Guan, X. yuan. Interleukin 17a Promotes Hepatocellular Carcinoma Metastasis via NF-KB Induced Matrix Metalloproteinases 2 and 9 Expression. *PLoS One* **2011**, *6* (7). https://doi.org/10.1371/journal.pone.0021816.

(59) Svinka, J.; Mikulits, W.; Eferl, R. STAT3 in Hepatocellular Carcinoma: New Perspectives. *Hepatic Oncol.* **2014**, *1* (1), 107–120. https://doi.org/10.2217/hep.13.7.

(60) Regis, G.; Pensa, S.; Boselli, D.; Novelli, F.; Poli, V. Ups and Downs: The STAT1:STAT3 Seesaw of Interferon and Gp130 Receptor Signalling. *Seminars in Cell and Developmental Biology*. Elsevier Ltd August 1, 2008, pp 351–359.

https://doi.org/10.1016/j.semcdb.2008.06.004.

(61) Fulmer, G. R.; M Miller, A. J.; Sherden, N. H.; Gottlieb, H. E.; Nudelman, A.; Stoltz, B. M.; Bercaw, J. E.; Goldberg, K. I.; Beckman, M. NMR Chemical Shifts of Trace Impurities: Common Laboratory Solvents, Organics, and Gases in Deuterated Solvents Relevant to the Organometallic Chemist. *Organometallics*. https://doi.org/10.1021/om100106e.